

## Geochemistry, Geophysics, Geosystems

### RESEARCH ARTICLE

10.1002/2014GC005486

#### Key Points:

- Hornblendite serves as the mantle source of orogenic alkali basalt
- Orogenic alkali basalts record recycling of subducted fossil oceanic crust

#### Supporting Information:

- Tables S1–S4

#### Correspondence to:

L.-Q. Dai,  
lqdai@ustc.edu.cn

#### Citation:

Dai, L.-Q., Z.-F. Zhao, and Y.-F. Zheng (2014), Geochemical insights into the role of metasomatic hornblendite in generating alkali basalts, *Geochem. Geophys. Geosyst.*, 15, 3762–3779, doi:10.1002/2014GC005486.

Received 7 JUL 2014

Accepted 5 SEP 2014

Accepted article online 13 SEP 2014

Published online 8 OCT 2014

Corrected 26 NOV 2014

This article was corrected on 26 NOV 2014. See the end of the full text for details.

### Geochemical insights into the role of metasomatic hornblendite in generating alkali basalts

Li-Qun Dai<sup>1</sup>, Zi-Fu Zhao<sup>1</sup>, and Yong-Fei Zheng<sup>1</sup>

<sup>1</sup>CAS Key Laboratory of Crust-Mantle Materials and Environments, School of Earth and Space Sciences, University of Science and Technology of China, Hefei, China

**Abstract** Experimental petrology suggested the role of hornblendite in generating alkali basalt. This mechanism is confirmed by an integrated study of major-trace elements and radiogenic isotopes for Mesozoic alkali basalts from the Qinling orogen in China. The alkali basalts have high contents of MgO (4.8–11.1 wt %, Mg# = 47–69), Na<sub>2</sub>O + K<sub>2</sub>O (2.9–5.4 wt %), TiO<sub>2</sub> (2.0–3.1 wt %) but low content of SiO<sub>2</sub> (41.4–49.6 wt %), which are generally silica-undersaturated with normative minerals of nepheline and olivine. They exhibit OIB-like trace element distribution patterns, with enrichment of LILE and LREE but no depletion of HFSE relative to the primitive mantle. They also show relatively depleted Sr-Nd-Hf isotope compositions, with low initial <sup>87</sup>Sr/<sup>86</sup>Sr ratios of 0.7028–0.7058, positive ε<sub>Nd</sub>(t) values of 4.0–9.8 and ε<sub>Hf</sub>(t) values of 8.8–13.5 for whole-rock, and positive ε<sub>Hf</sub>(t) values of 5.2–16.4 for zircon. Such element and isotope features indicate their origination from the juvenile subcontinental lithospheric mantle (SCLM) source with involvement of crustal components. The alkali basalts generally have high K<sub>2</sub>O/Na<sub>2</sub>O ratios, and high K<sub>2</sub>O and TiO<sub>2</sub> contents, suggesting their derivation from partial melting of hornblendite-rich mantle lithology. They also exhibit variable K/La and Ti/La ratios that are correlated with (La/Yb)<sub>N</sub> ratios, indicating a geochemical heterogeneity of the SCLM source. Taken together, all the above geochemical features can be accounted for by partial melting of a hornblendite-rich SCLM source. The hornblendite would be generated by reaction of the juvenile SCLM wedge peridotite with hydrous felsic melts derived from subducted Palaeotethyan oceanic crust at the slab-mantle interface in the subduction channel. Therefore, orogenic alkali basalts record recycling of the subducted fossil oceanic crust, and the metasomatic hornblendite is an important lithology in local SCLM domains above fossil subduction channels.

### 1. Introduction

Alkali basalts commonly occur in the interior of plate, typically on updomed and rifted continental crust (continental intraplate basalts) and on oceanic islands (OIB). They are generally characterized by high contents of alkali metals and normative nepheline in their CIPW norms [Hofmann, 1997; Niu and O'Hara, 2003; Niu, 2008; Pilet et al., 2008, 2011; Ma et al., 2011]. Extensive geochemical and petrological studies have been taken on the origin of alkali oceanic basalts, dealing with both natural samples and laboratory experiments [e.g., Hirschmann et al., 2003; Dasgupta et al., 2007; Pilet et al., 2008; Niu et al., 2011]. Considerable evidence has been accumulated, demonstrating that the mantle source of some alkali basalts contain crustal components that were derived from recycling of subducted oceanic crust [e.g., Hofmann, 1997; Zhang et al., 2009; Stracke, 2012]. However, the nature of mantle sources, especially the mantle lithology, for the alkali basalts still remains enigmatic. Although low-degree partial melting of peridotite at high pressure could produce alkali melts [Takahashi and Kushiro, 1983], the majority of experimentally produced mafic melts from the peridotite are not similar to natural alkali basalts, because the experimental products show significantly lower CaO and higher Al<sub>2</sub>O<sub>3</sub> contents than natural alkali basalts [e.g., Hirschmann et al., 2003; Dasgupta et al., 2007]. Besides peridotite, metasomatic lithologies such as carbonated peridotite, pyroxenite, and hornblendite have been suggested as the mantle source of some OIB [e.g., Sobolev et al., 2005, Sobolev et al., 2011; Dasgupta et al., 2007; Pilet et al., 2008; Herzberg, 2011]. Although experimental petrological studies suggested the role of metasomatic lithologies in generating the alkali basalts, geochemical evidence from natural samples supporting this mechanism is limited. Therefore, the major issue for the petrogenesis of alkali basalts is to recognize the contribution from different mantle lithologies and their origin [Sobolev et al., 2005; Niu, 2008; Pilet et al., 2008, 2011].

There are also alkali basalts above fossil subduction zones, but little attention has been paid to their petrogenesis. Although these fossil subduction zones have evolved into collisional orogens, a genetic link between alkali basalts and their mantle sources is still unknown in both petrology and geochemistry. As such, orogenic alkali basalts provide us with an excellent opportunity to investigate the nature of subcontinental lithospheric mantle (SCLM) above fossil subduction zones. Partial melting of subducting oceanic crust and its subsequent melt-peridotite interaction has been considered the important process in oceanic subduction channel [Ringwood, 1990; Zheng, 2012]. The melt-peridotite reaction can generate ultramafic metasomes with different lithologies such as pyroxenite and hornblendite [e.g., Yaxley and Green, 1998; Prouteau *et al.*, 2001; Pertermann and Hirschmann, 2003; Rapp *et al.*, 2010]. Metasomatic veins rich in hornblende and pyroxene are also observed in many mantle-derived xenoliths [Malaspina *et al.*, 2006; Coltorti *et al.*, 2007; Downes, 2007]. Such metasomes may serve as the mantle sources of alkali basalts because they bear the geochemical signatures of not only the mantle wedge but also the subducting crust. However, there are differential contributions in the composition of major and trace elements from the mantle and crustal rocks to the mantle sources. While the SCLM wedge peridotite was directly reacted with metasomatic agents, the metasomatic agents would occur in the form of felsic melts rather than crustal rocks themselves [Zhang *et al.*, 2009; Zhao *et al.*, 2013]. As such, the crustal components in the mantle source cannot be directly represented by the subducted oceanic crust.

In this contribution, we present a combined study of whole-rock major-trace elements and Sr-Nd-Hf isotopes as well as zircon U-Pb ages and Lu-Hf isotopes for Mesozoic alkali basalts from the Qinling orogen in central China. The results provide new insights not only into the role of metasomatic hornblendite in generating the mantle source of alkali basalts but also into the recycling of subducted Palaeotethyan oceanic crust. Consequently, we conclude that the metasomatic hornblendite was generated by reaction of the overlying juvenile SCLM peridotite with hydrous felsic melts derived from the subducted Palaeotethyan oceanic crust in the fossil subduction channel. Partial melting of the metasomatic hornblendite together with minor host peridotite gives rise to the alkali basalts in West Qinling.

## 2. Geological Setting and Samples

The Qinling-Tongbai-Hong'an-Dabie-Sulu orogenic belt marks the final amalgamation between the North China Block (NCB) and the South China block (SCB) in central China [Wu and Zheng, 2013]. To the east, the Dabie-Sulu orogens were built by continent-continent collision in the Mesozoic. To the west, the Qinling-Tongbai-Hong'an orogens was produced by a series of accretionary-type arc-continent collision orogeny in the Paleozoic with the final continent-continent collision orogeny in the Mesozoic. This composite orogenic belt involves a series of tectonic processes from the subduction of oceanic crust in the Paleozoic to the subduction of continental crust in the Mesozoic [Zheng *et al.*, 2013].

The Qinling orogen is tectonically bounded by the Qilian orogen to the northwest and the North China Block to the north, the Songpan-Ganzi orogen, and the South China Block to the south, the Kunlun orogen to the southwest, and the Hong'an orogen to the east (Figures 1a and 1b). It can be subdivided into the East Qinling orogen and the West Qinling orogen (Figure 1b) by the Baoji-Chengdu railway [Zhang *et al.*, 2001, 2007]. The East Qinling orogen can be further subdivided into North Qinling and South Qinling by the Shangdan fault [Meng and Zhang, 2000; Zhang *et al.*, 2001]. North Qinling is mainly composed of Neoproterozoic to Early Paleozoic medium-grade to high-grade metasedimentary and metavolcanic rocks, including the Qinling Complex, Kuanping, and Erlangping groups [Li *et al.*, 1993; Dong *et al.*, 2011]. South Qinling is dominated by Late Paleozoic to Triassic medium-grade metasedimentary and metavolcanic rocks [Li *et al.*, 1993; Meng and Zhang, 1999; Zhu *et al.*, 2011]. The closure of Shangdan Paleotethys is assumed to occur in the middle Paleozoic, resulting in the arc-continent collision between North Qinling and South Qinling [Hacker *et al.*, 2004; Dong *et al.*, 2011; Wu and Zheng, 2013]. The A'nimaque-Mianlue fault along the southern margin of the Qinling orogen represents the closure of A'nimaque-Mianlue Paleotethyan sea, which was located in the north to the Songpan-Ganzi orogen and the South China Block during the Late Paleozoic [Dong *et al.*, 2011; Wu and Zheng, 2013]. With the northward subduction of the A'nimaque-Mianlue Paleotethyan oceanic crust, the arc-continent collision between the South Qinling and the South China Block occurred in the Triassic, leading to the final amalgamation between the North China block and the South China Block [Meng and Zhang, 2000; Meng *et al.*, 2005; Dong *et al.*, 2011].

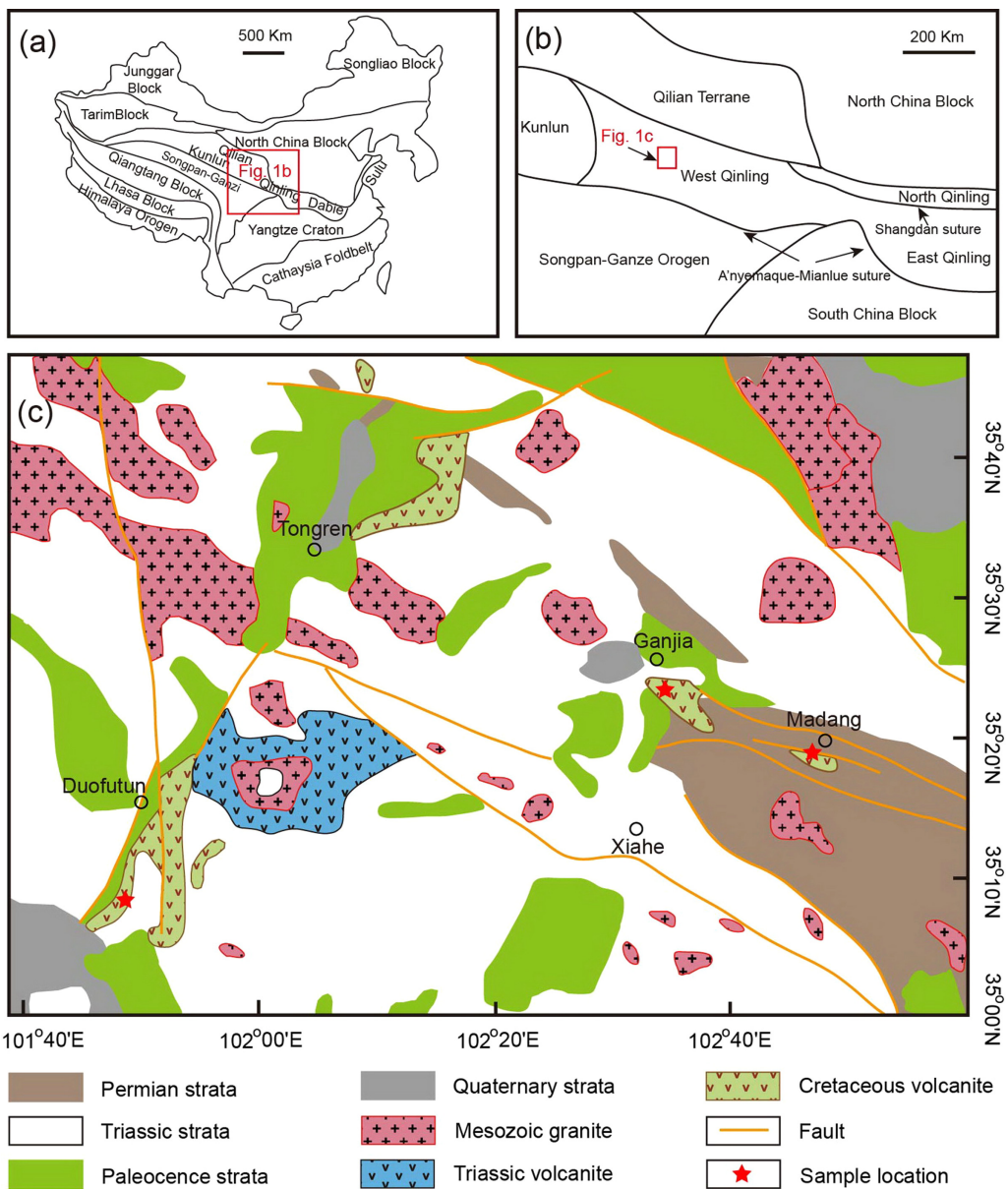


**Figure 1.** (a) Simplified tectonic map showing major cratonic blocks and orogenic belts in China [modified after Zheng *et al.*, 2013]; (b) geological map of the major tectonic units around West Qinling; (c) simplified geological map showing the distributions of Early Cretaceous alkali basalts [modified after Zhang *et al.*, 1992].

In the West Qinling orogen, sedimentary cover is mainly composed of Devonian to Cretaceous sediments, with rarely exposed Precambrian crystalline basement [Feng *et al.*, 2002]. The oldest exposed crystalline basement in the West Qinling orogen is the Qinling Group, which predominantly consists of gneisses, amphibolites, and marbles, with Paleoproterozoic zircon U-Pb ages of 2.17–2.27 Ga [Meng and Zhang, 2000; Dong *et al.*, 2011]. Voluminous granitoids rocks of Late Triassic were emplaced in West Qinling [Lu, 1999; Dong *et al.*, 2011; Wang *et al.*, 2011a, 2013]. There are also sporadic volcanic rocks, mainly composed of melilitite, alkali basalt, andesite, rhyolite, and carbonatite, erupted in West Qinling during the Late Triassic, Late Cretaceous, and Cenozoic periods [Li *et al.*, 2013a, 2013b; Yu *et al.*, 2011]. These volcanic rocks, especially the basalt and carbonatite, provide us with a good opportunity to investigate the nature of subcontinental lithospheric mantle in the Qinling orogen.

Voluminous igneous rocks were emplaced in the Qinling orogen, which are mainly composed of massive granitoids, with sporadic volcanic rocks and lamprophyre dykes [Lu, 1999; Zhang *et al.*, 2008;

*Wang et al.*, 2007, 2013]. In particular, there are sporadic occurrences of Early Cretaceous to Cenozoic alkali basalts in the West Qinling orogen [*Qin et al.*, 2008, 2009; *Li et al.*, 2013a; *Yu et al.*, 2011], together with voluminous granitoids of Late Triassic [*Dong et al.*, 2011; *Wu and Zheng*, 2013]. While numerous studies have been devoted to the Late Triassic granitoids [*Qin et al.*, 2008, 2009; *Wang et al.*, 2011a, 2011b], less attention has been paid to the Early Cretaceous alkali basalts in the West Qinling orogen [*Ding et al.*, 2013; *Li et al.*, 2013a]. Based on relatively depleted radiogenic Sr-Nd isotope compositions, these alkali basalts were interpreted as derivation from the asthenospheric mantle [*Fan et al.*, 2007a, 2007b; *Ding et al.*, 2013; *Li et al.*, 2013a]. However, these alkali basalts generally exhibit enrichment of melt-mobile incompatible trace elements such as light rare earth elements (LREE) and large ion lithophile elements (LILE) relative to normal mid-ocean ridge basalts (MORB), a typical product derived from partial melting of the normal asthenospheric mantle-derived melts. Therefore, the nature of the mantle source for these alkali basalts is still unclear.

Basalt samples used in this study were collected from the Madang, Ganjia, and Duomahe areas, three major Early Cretaceous volcanic rocks in the West Qinling orogen (Figure 1c). The Madang volcanic rocks outcrop as a small W-E extended hillock with an area of  $\sim 0.5 \text{ km}^2$ , about 30 km to the northeast of Xiale county. They are unconformably over the Permian strata and below the Neogene strata, with  $\sim 300 \text{ m}$  thick [*Fan et al.*, 2007a; *Ding et al.*, 2013]. The Madang volcanic rocks are mainly composed of basalt and andesite. And the studied basalts are porphyritic texture, and composed of plagioclase and clinopyroxene phenocrysts. The Ganjia basalts outcrop in Ganjia town, about 25 km to the north of Xiale county. They are also unconformably over the Permian strata, with olivine and minor plagioclase phenocrysts. Olivine phenocrysts are subhedral to anhedral, most of them show fractures. Some of the olivine phenocrysts were partially altered to iddingsite at rims and fractures. The Duomahe volcanic rocks mainly occur along the N-S extended basin with an area of  $\sim 90 \text{ km}^2$  (Figure 1c), locally unconformably overlay the Triassic strata. They mainly consist of basalt with minor basaltic andesite. Duomahe volcanic rocks used in study were basalts, collecting from Duomahe town. These basalts have phenocrysts of olivine, minor plagioclase and clinopyroxene.

### 3. Analytical Methods

#### 3.1. Whole-Rock Major-Trace Elements

After petrographic examination, 18 fresh samples were selected, crushed to powders of 200 meshes in agate mortars. Whole-rock major elements were measured on fused glass discs by X-ray fluorescence spectrometer (XRF) at ALS Chemex Company (Guangzhou, China). Analytical precision is better than 2–5%, estimated from repeated analyses of two standards (diorite gneiss SY-4 and basalt GSE-3). Trace elements were analyzed using Agilent 7500a ICP-MS after complete dissolution at State Key Laboratory of Geological Processes and Mineral Resources in China University of Geosciences, Wuhan. The powders ( $\sim 50 \text{ mg}$ ) were digested by  $\text{HF} + \text{HNO}_3$  in Teflon bombs at  $190^\circ\text{C}$  for 12 h. The detailed sample-digesting procedure for ICP-MS analyses are the same as description by *Liu et al.* [2008a]. Four standards (andesite AGV-2, rhyolite RGM-2, basalt BCR-2, and BHVO-2) were used to monitor the analytical quality, and the analytical precision for most trace elements is better than  $\pm 5\%$ .

#### 3.2. Whole-Rock Sr-Nd-Hf Isotopes

Whole-rock Rb-Sr, Sm-Nd, and Lu-Hf isotopic analyses were performed on a Thermo Scientific Neptune MC-ICP-MS at State Key Laboratory of Lithospheric Evolution in Institute of Geology and Geophysics, Chinese Academy of Sciences (CAS), Beijing. Detailed separation, purification, and measure procedures for Rb-Sr, Sm-Nd, and Lu-Hf isotopic analyses from one sample digestion was used, as described in detail by *Yang et al.* [2010, 2011a, 2011b]. The whole-rock powders ( $\sim 100 \text{ mg}$ ) were weighed, and dissolved in Teflon capsules with  $\text{HF} + \text{HNO}_3 + \text{HClO}_4$  at  $190^\circ\text{C}$  for a week. The first stage was the separation and purification of Hf using Eichrom Ln-spec resin ( $100\text{--}150 \mu\text{m}$ , 2 mL), modified from the procedure of *Münker et al.* [2001]. The second stage involved standard cation exchange chromatography for Rb and Sr purification, and the Sr fraction was further purified by Sr-specific resin [*Balcaen et al.*, 2005; *Yang et al.*, 2012]. Finally, REE were eluted after the separation of Sr and further purified using another Eichrom Ln resin ( $100\text{--}150 \mu\text{m}$ , 2 mL) for Nd. The total procedural blanks for Hf, Sr, and Nd are less than 50 pg, 100 pg, and 50 pg, respectively. The  $^{87}\text{Sr}/^{86}\text{Sr}$ ,  $^{143}\text{Nd}/^{144}\text{Nd}$ , and  $^{176}\text{Hf}/^{177}\text{Hf}$  ratios were normalized to  $^{86}\text{Sr}/^{88}\text{Sr} = 0.1194$ ,  $^{146}\text{Nd}/^{144}\text{Nd} = 0.7219$ , and  $^{179}\text{Hf}/^{177}\text{Hf} = 0.7325$ , respectively, using the exponential law. Analytic precisions of isotopic ratio

measurements are given as  $2\sigma$  standard errors. During our analyses, USGS reference material BCR-2 was also processed for Sr-Nd-Hf isotopes, and gave ratios of  $0.7050003 \pm 23$  for  $^{87}\text{Sr}/^{86}\text{Sr}$ ,  $0.512636 \pm 9$  for  $^{143}\text{Nd}/^{144}\text{Nd}$ , and  $0.282850 \pm 5$  for  $^{176}\text{Hf}/^{177}\text{Hf}$ , respectively, which are identical within errors, to the recommended values [Weis *et al.*, 2006, 2007].

### 3.3. Zircon U-Pb Dating

Zircon was separated by the standard density and magnetic separation techniques, and then selected by hand picking under a binocular microscope. Representative zircon grains were mounted in epoxy resin, and then polished to exposed grain center. As a guide to the selection of in situ analysis spot, transmitted and reflected light micrographs as well as cathodoluminescence (CL) were taken to reveal their external morphology and internal structure. The CL images were obtained using JSM-6700F scanning electron microscope in University of Science and Technology of China (USTC) at Hefei.

Zircon U-Pb dating was conducted by LA-ICP-MS at State Key Laboratory of Geological Processes and Mineral Resources in China University of Geosciences, Wuhan. Detailed operating conditions for the laser ablation system and the ICP-MS instrument and data reduction are the same as description by Liu *et al.* [2008b, 2010]. An Agilent 7500a ICP-MS instrument was used to acquire ion-signal intensities. Helium was applied as a carrier gas. Argon was used as the makeup gas and mixed with the carrier gas via a T-connector before entering the ICP. Analyses of the zircons were conducted with a laser repetition rate of 6 Hz and beam diameter of  $32 \mu\text{m}$ . Off-line selection and integration of background and analyte signals, and time-drift correction and quantitative calibration for trace element analyses and U-Pb dating were performed by ICPMS-DataCal [Liu *et al.*, 2008b, 2010]. Zircon 91500 was used as external standard for U-Pb dating, and was analyzed twice every five analyses. Preferred U-Th-Pb isotopic ratios used for 91500 are from Wiedenbeck *et al.* [1995]. U-Pb concordia diagrams and weighted mean calculations are made using Isoplot/Ex\_ver3.23 [Ludwig, 2003].

### 3.4. Zircon Lu-Hf Isotopes

After the LA-ICP-MS zircon U-Pb dating, the in situ measurement of zircon Lu-Hf isotopes was performed on a Neptune MC-ICP-MS at State Key Laboratory of Lithospheric Evolution in Institute of Geology and Geophysics, CAS, Beijing. The instrumental conditions and data acquisition were described by Xu *et al.* [2004] and Wu *et al.* [2006]. The analyses were conducted with a beam diameter of  $60 \mu\text{m}$ , 8 Hz repetition rate, and a laser power of 100 mJ/pulse. The isobaric interference of  $^{176}\text{Lu}$  and  $^{176}\text{Yb}$  on  $^{176}\text{Hf}$  was corrected following the method described in Izuka and Hirata [2005]. During the analysis, standard zircons gave  $^{176}\text{Hf}/^{177}\text{Hf}$  ratios of  $0.2825105 \pm 0.000003$  ( $2\sigma$ ,  $n = 52$ ) for Mud Tank and  $0.282021 \pm 0.000006$  ( $2\sigma$ ,  $n = 29$ ) for GJ-1. They are all consistent within analytical errors with the recommended  $^{176}\text{Hf}/^{177}\text{Hf}$  ratios of  $0.282507 \pm 0.000006$  for Mud Tank [Woodhead and Hergt, 2005] and  $0.282015 \pm 0.000019$  for GJ-1 [Elhlou *et al.*, 2006], respectively. The  $^{176}\text{Lu}$  decay constant of  $1.865 \times 10^{-11} \text{ year}^{-1}$  was adopted [Scherer *et al.*, 2001]. Initial  $^{176}\text{Hf}/^{177}\text{Hf}$  ratios were calculated with reference to the chondritic reservoir (CHUR) of Blichert-Toft and Albarède [1997] at the time of zircon growth from magma. And single-stage Hf model ages ( $T_{\text{DM1}}$ ) are calculated relative to the depleted mantle with present-day  $^{176}\text{Hf}/^{177}\text{Hf} = 0.28325$  and  $^{176}\text{Lu}/^{177}\text{Hf} = 0.0384$  [Griffin *et al.*, 2000].

## 4. Results

In order to decipher the origin of alkali basalts in the West Qinling orogen, we have extended the geochemical data from those analyzed in this study to those in the literature. As a consequence, a comprehensive compilation of geochemical data is available for the alkali basalts in the target area (supporting information Tables S1–S3). The data are primarily composed of zircon U-Pb ages, whole-rock Ar/Ar ages, whole-rock major-trace elements and Sr-Nd-Hf isotopes, and zircon Lu-Hf isotopes.

There are only a very small amount of zircon grains that were separated in this study from the West Qinling alkali basalts. For sample 12LZ14 at Ganjia, about 150 zircon grains were separated from  $>20 \text{ kg}$  basalt sample, which were selected for the LA-ICP-MS U-Pb dating. The zircon U-Pb isotope data are presented in supporting information Table S1 and the CL images of representative zircon grains are illustrated in Figure 2a. Generally, zircon grains from the basalt are anhedral, and have grain sizes of  $100\text{--}400 \mu\text{m}$ . Most zircon grains are characterized by banded zoning in CL images. As shown in Figure 2b, zircon U-Pb isotope data

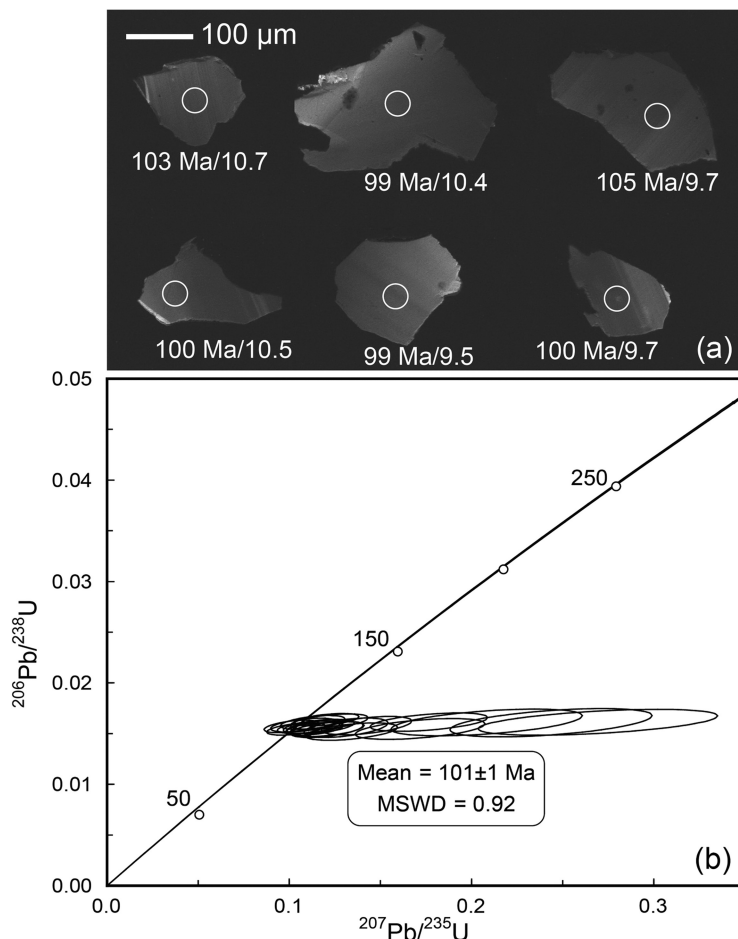


**Figure 2.** (a) CL images of representative zircons and (b) concordia diagrams of zircon LA-ICPMS U-Pb isotope data for alkali basalts from Ganja in West Qinling, indicating an eruptive age of  $101 \pm 1$  Ma for the Ganja basalt. Circles in Figure 2a denote the analytical spots, together with zircon U-Pb ages/ $\varepsilon_{\text{Nd}}(\text{t})$  values. The scale bar is  $100 \mu\text{m}$ .

Therefore, the Early Cretaceous alkali basalts in the West Qinling orogen mainly erupted at 101–112 Ma. They are remarkably later than the Triassic continental collision, indicating their formation in the postcollisional stage.

According to the nomenclature of *Le Bas et al.* [1986], all of the alkali basalts fall in the domain of basanite and basalt in the total alkalis versus  $\text{SiO}_2$  diagram (Figure 3). In the terms of CIPW normative calculations, most of the basalts have normative nepheline + olivine, with minor samples that contain normative olivine + hypersthene. Therefore, the study samples are silica-undersaturated alkali basalts. These alkali basalts generally have  $\text{SiO}_2$  contents of 41.4–49.6 wt % (supporting information Table S2), exhibiting high contents of  $\text{MgO}$  (4.8–11.1 wt %,  $\text{Mg}^{\#} = 47$ –69),  $\text{Na}_2\text{O} + \text{K}_2\text{O}$  (2.9–5.4 wt %) and  $\text{TiO}_2$  (2.0–3.1 wt %). They exhibit moderate LREE enrichment in the chondrite-normalized REE distribution diagram (Figure 4a), similar to common patterns for oceanic island basalts (OIB). All the alkali basalts have no significant Eu anomaly, suggesting that plagioclase is not a major fractionating phase. On the primitive mantle-normalized trace element spidergram (Figure 4b), the basalts exhibit enrichment of LILE, no depletion of high field strength elements (HFSE) such as Nb and Ta, and negative Pb anomalies (Figure 5b), also similar to common patterns for OIB. Nevertheless, they have lower Rb abundances than OIB and positive Sr anomalies; some samples exhibit positive Pb and K positive anomalies.

For radiogenic isotopes, these alkali basalts generally have initial  $^{87}\text{Sr}/^{86}\text{Sr}$  ratios of 0.7028–0.7058 (Figure 5 and supporting information Table S2),  $\varepsilon_{\text{Nd}}(\text{t})$  values of 4.0–9.8 and  $\varepsilon_{\text{Hf}}(\text{t})$  values of 8.8–13.6 for whole-rock. Single-stage Nd and Hf model ages for the basalts range from 136 to 625 Ma and 256 to 459 Ma, respectively (supporting information Table S2). Twenty analyses for the zircons from the Ganja basalt 12LZ14 yield positive

for 20 analyses yield a weighted  $^{206}\text{Pb}/^{238}\text{U}$  age of  $101 \pm 1$  Ma ( $\text{MSWD} = 0.92$ ) for the Ganja basalt. These zircon grains exhibit high Th/U ratios of 0.13–0.83 (supporting information Table S1) and significant oscillatory zoning (Figure 2a), indicating magmatic origin. Therefore, our new zircon U-Pb dating yields the eruptive age for the Ganja basalt, which is at the boundary between Early and Late Cretaceous (supporting information Table S1 and Figure 2b). This is the first report for the eruption age of alkali basalts in the Ganja area. Previous geochronological studies yield a whole-rock Ar/Ar age of  $112 \pm 1$  Ma (supporting information Table S2) [*Fan et al.*, 2007a] and zircon U-Pb ages of 103–106 Ma (supporting information Table S1) [*Li et al.*, 2013a] for the Duomohe basalts, and a zircon U-Pb age of 105 Ma for the Madang alkali basalts (supporting information Table S1) [*Ding et al.*, 2013]. There-

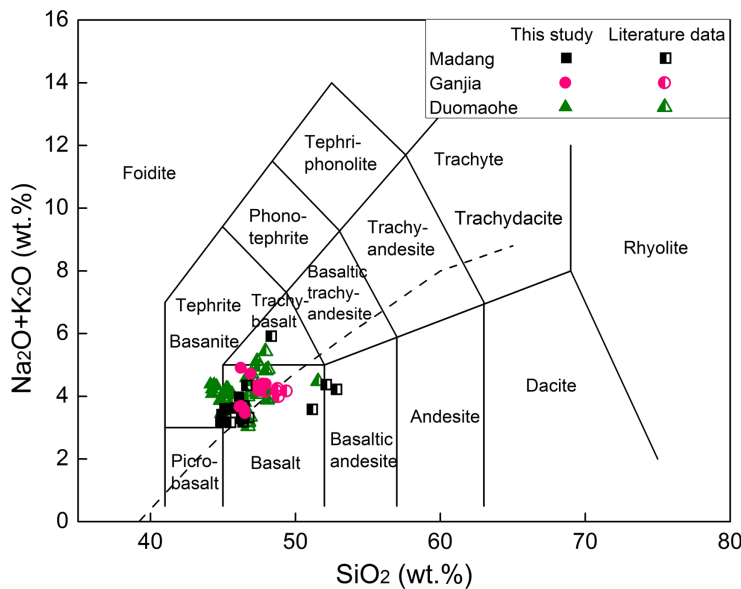


**Figure 3.** Total alkali versus  $\text{SiO}_2$  (TAS) diagram for alkali basalts from West Qinling. The classification is after Le Bas et al. [1986]. Data source: this study, Fan et al. [2007a, 2007b], Yan et al. [2012], Ding et al. [2013], and Li et al. [2013a].

which is fertile in lithochemistry, enriched in melt-mobile incompatible trace elements but depleted in radiogenic isotopes.

## 5. The Origin of Alkali Basalts

The mass balance between major-trace elements and stable-radiogenic isotopes must be taken into account in any model of basalt petrogenesis. For major elements, the alkali basalts from the West Qinling orogen certainly require the mantle source of ultramafic lithology such as peridotite, pyroxenite, and hornblendite, or their combination in different proportions. For trace elements, the alkali basalts are characterized by enrichment of melt-mobile incompatible elements such as LILE and LREE, no depletion of Nb and Ta, and mostly negative Pb anomalies; their trace element distribution patterns are similar to common OIB but significantly different from MORB in the spidergram (Figures 4a and 4b). This indicates involvement of crustal components in their mantle source. For radiogenic isotope compositions, they generally have high initial  $^{87}\text{Sr}/^{86}\text{Sr}$  ratios and positive  $\varepsilon_{\text{Nd}}(t)$  values, resembling common MORB (Figure 5) and thus suggesting involvement of the asthenospheric component in the mantle source. Taken together, the mantle source of alkali basalts contains not only the crustal components that are rich in melt-mobile incompatible trace elements but also the mantle component that is isotopically depleted relative to the bulk silicate Earth.

### 5.1. Constraints From Major Elements

Numerous experimental studies have been taken to study the origin of alkali basalts [e.g., Walter, 1998; Hirschmann et al., 2003; Dasgupta et al., 2007; Pilet et al., 2008]. It is well known that low-degree partial melting of peridotite at high pressure can generate mafic melts that are strongly enriched in alkali [e.g., Hirose and Kushiro, 1993; Takahashi and Kushiro, 1983; Walter, 1998]. However, these experimentally produced melts are generally too high in  $\text{SiO}_2$  and  $\text{Al}_2\text{O}_3$  contents, but too low in  $\text{CaO}$  contents compared to common OIB of alkalic composition [e.g., Hirschmann et al., 2003; Dasgupta et al., 2007]. Therefore, it is well accepted that the partial melting of pure peridotite cannot account for the lithochemical feature of alkali basalts on Earth [Hirschmann et al., 2003; Dasgupta et al., 2007; Niu, 2008]. The experimentally produced melts of peridotite generally have high  $\text{SiO}_2$  contents of 45–54 wt % [e.g., Kushiro, 1996; Walter, 1998; Wasylewski et al., 2003], whereas the alkali basalts from the West Qinling orogen exhibit low  $\text{SiO}_2$  contents of 41.4–49.6 wt % (supporting information Table S2). This difference also suggests that they cannot be produced by the partial melting of pure peridotite.

According to partial melting experiments, the following ultramafic lithologies have been considered as the mantle source of silica-undersaturated alkali melts: (1) carbonated peridotite [Hirose, 1997; Dasgupta et al.,

$\varepsilon_{\text{Hf}}(t)$  values of 5.9–12.1 (Figure 6a and supporting information Table S3), with single-stage Hf model ages of 315–594 Ma (Figure 6b). Zircons from Duomaohhe basalts also yield positive  $\varepsilon_{\text{Hf}}(t)$  values of 5.2–16.4 (Figure 6a) [Li et al., 2013a], with single-stage Hf model ages of 132–578 Ma (Figure 6b). Most of the zircon  $\varepsilon_{\text{Hf}}(t)$  values and the single-stage Hf model ages are within the ranges of whole-rock  $\varepsilon_{\text{Hf}}(t)$  values and Hf model ages.

As a general view, all these geochemical features indicate that the alkali basalts would be derived from a kind of ultramafic lithologies,

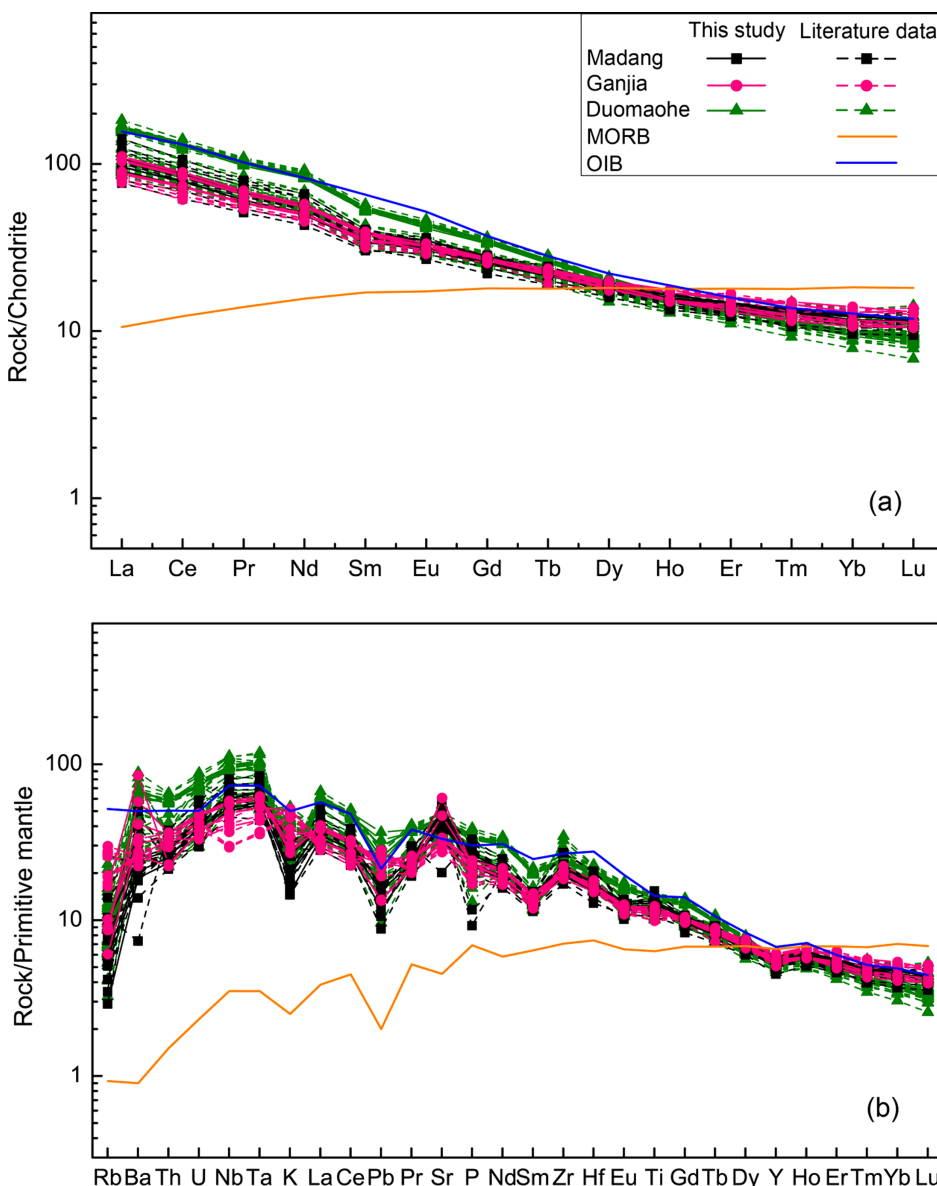


**Figure 4.** Whole-rock geochemical diagrams for alkali basalts from West Qinling. (a) Chondrite-normalized REE patterns, displaying the enrichment of LREE relative to HREE; (b) primitive mantle-normalized trace element distribution patterns, displaying the enrichment of LILE but no depletion of HFSE such as Nb and Ta, with Pb negative anomaly, similar to common patterns for OIB. Data sources for the West Qinling alkali basalts: this study, *Fan et al.* [2007a, 2007b], *Yan et al.* [2012], *Ding et al.* [2013], and *Li et al.* [2013a]. The chondrite and primitive mantle data are from *McDonough and Sun* [1995]. MORB and OIB compositions are after *Sun and McDonough* [1989].

2007]; (2) silica-deficient eclogite or garnet pyroxenite [e.g., *Hirschmann et al.*, 2003; *Kogiso et al.*, 2003, 2004]; (3) metasomatic hornblendite [*Pilet et al.*, 2008, 2011]. The silica-undersaturated alkali basalts from the West Qinling have high MgO (up to 11.1 wt %, most of which >7.5 wt %) and low SiO<sub>2</sub> (41.4–49.6 wt%) contents, suggesting the limited evolution of mantle-derived mafic magma. A comparison of the alkali basalts with the experimental melts from these three possible mantle sources delineated in Figure 7 may be insightful.

Melting experiments on carbonated peridotite suggest that the major element compositions of alkali basalts can be produced by low-degree partial melting of lherzolites (fertile peridotites) with the addition of CO<sub>2</sub> [*Hirose*, 1997; *Dasgupta et al.*, 2007]. Although the CaO contents of alkali basalts from West Qinling are within the range of carbonated peridotite-derived melts, other major elements are all beyond the ranges of those from the carbonated peridotite-derived melts, especially the significantly high TiO<sub>2</sub> and alkali

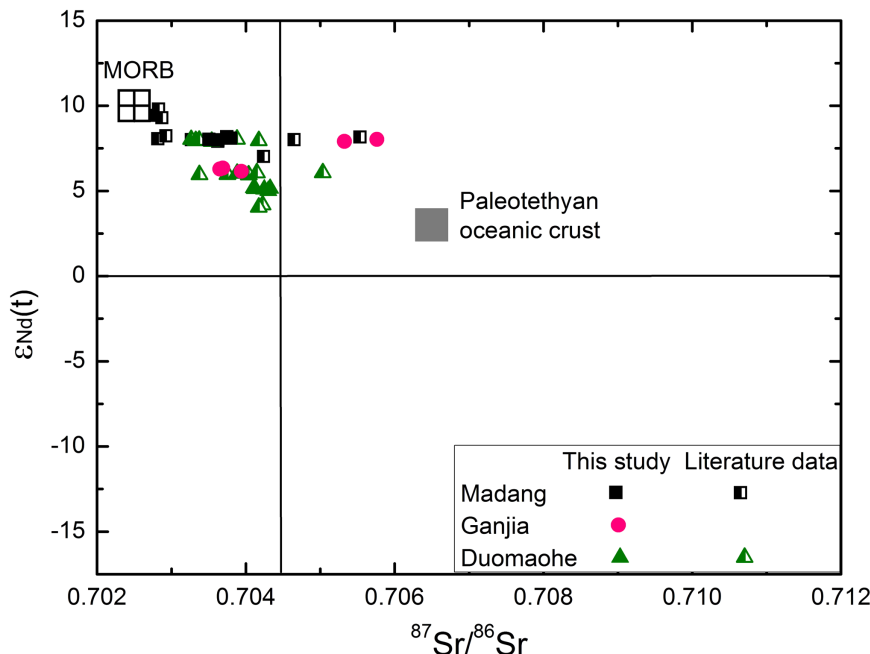


**Figure 5.** Initial Sr and Nd isotope ratios for Mesozoic alkali basalts from West Qinling, showing relatively depleted whole-rock Sr-Nd isotope compositions. Data sources for the West Qinling alkali basalts: this study, *Fan et al.* [2007a, 2007b], *Ding et al.* [2013], and *Li et al.* [2013a]. Also compared are those of eclogites with geochemical affinities to Paleotethyan oceanic crust [*Fu et al.*, 2002] and MORB [*Ito et al.*, 1987]. All these data are recalculated at  $t = 101$  Ma.

contents (Figures 7a, 7b, and 7d). *Prytulak and Elliott* [2007] suggest that peridotite has insufficient Ti to reproduce the compositions of many alkali OIB, and a Ti-rich material is a necessary additive to the peridotite. Thus, the carbonated peridotite is not suitable as the mantle source of alkali basalts from West Qinling.

Silica-deficient pyroxenite also has been considered as the mantle source of alkali basalts, whereas silica-excess pyroxenite is regarded as the mantle source of tholeiitic basalts [e.g., *Hirschmann et al.*, 2003; *Keshav et al.*, 2004; *Zhang et al.*, 2009]. However, high pressure partial melting of silica-deficient pyroxenite generally have much lower  $K_2O$  content and  $K_2O/Na_2O$  ratios (Figures 7b and 7c) than the West Qinling alkali basalts, although they can produce Ne-normative melts. *Pilet et al.* [2008] also suggested that the high  $K_2O$  contents of alkali basalts cannot be explained by silica-deficient pyroxenite as a source, either dry or with  $CO_2$ . Therefore, the silica-deficient pyroxenite also cannot explain the major elements in the alkali basalts from West Qinling.

Partial melting of hornblendite, Cpx hornblendite, and hornblendite + peridotite sandwich can generate mafic melts that generally have high alkali contents and  $K_2O/Na_2O$  ratios, plotting relatively close to the alkali basalts from West Qinling (Figure 7). In particular, partial melting of the hornblendite + peridotite sandwich can produce the mafic melts of high  $SiO_2$  contents that are very close to the alkali basalts from West Qinling for all the major elements. On the other hand, the pure hornblendite-derived melts have too low  $SiO_2$  contents compared to the alkali basalts from West Qinling. In this regard, the hornblendite + peridotite sandwich most likely represents the mantle lithology of alkali basalts from West Qinling in view of the available studies from experimental petrology.

Experimental studies of Fe/Zn partition coefficients ( $D_{Fe/Zn}$ ) between mineral and melt indicate that  $D_{Fe/Zn}$  is  $\sim 1$  to 1.1 for olivine and orthopyroxene, but  $>>1$  for clinopyroxene, garnet and amphibole [*Le Roux et al.*, 2010, 2011; *Lee et al.*, 2010]. Thus, pyroxenite/hornblendite-derived melts would have lower Fe/Zn ratios than those of peridotite-derived melts [*Le Roux et al.*, 2011]. As shown in supporting information Table S2, the alkali basalts have Fe/Zn ratios of 346–1444, about half of which lower than the 930–1200 for MORB [*Le Roux et al.*, 2010]. Thus, the low Fe/Zn ratios probably indicate the contribution from pyroxenite/hornblendite-rich mantle lithology to their mantle source. However, there are significantly high contents of  $K_2O$  (0.43–1.5 wt %) and  $TiO_2$  (2.0–3.1 wt %) in the alkali basalts from West Qinling (supporting information Table S2). This requires the presence of K-rich and Ti-rich components in the mantle source, which can be

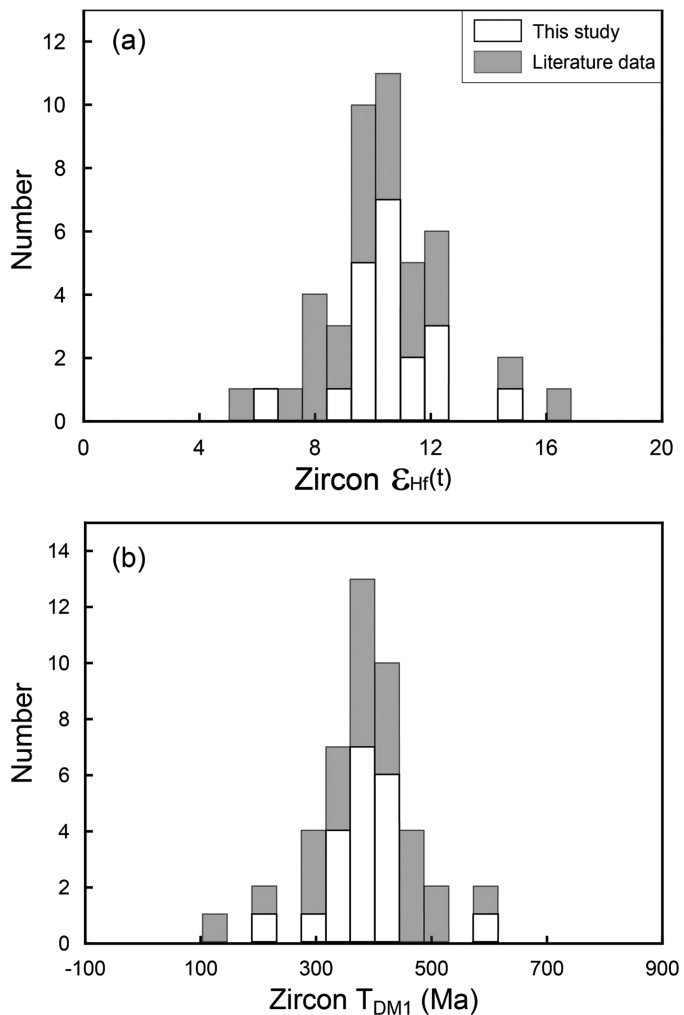


**Figure 6.** (a) Histogram of zircon  $\epsilon_{\text{Nd}}(t)$  values and (b) single-stage Hf model ages for alkali basalts from West Qinling, showing positive zircon  $\epsilon_{\text{Nd}}(t)$  values and young zircon Hf model ages. Data sources: this study and Li *et al.* [2013a].

hydrous melt-peridotite reaction [Rapp *et al.*, 1999; Prouteau *et al.*, 2001], and they are often observed in many mantle-derived xenoliths [e.g., Downes *et al.*, 2004; Powell *et al.*, 2004; Coltorti *et al.*, 2007]. In this regard, the alkali basalts from West Qinling would be likely derived from partial melting of the hornblende-rich metasomatic veins in the mantle wedge peridotite. Because hornblende vein-derived melts are strongly silica-undersaturated, they might react with orthopyroxene in the host peridotite to generate relatively high-silica mafic melts plus olivine [Hirschmann *et al.*, 2003; Pilet *et al.*, 2008]. There are variable SiO<sub>2</sub> contents for the alkali basalts from West Qinling, with several samples that do not contain normative nepheline. This may result from the reaction of silica-undersaturated melts with peridotite. Therefore, the hornblende vein + peridotite sandwich may be the most likely lithologies for the mantle source of alkali basalts from West Qinling.

### 5.2. Constraints From Trace Element and Isotope Compositions

On the chondrite-normalized and primitive mantle-normalized trace element diagrams (Figure 4), the alkali basalts from West Qinling are characterized by enrichment of LREE and LILE but no depletion of such HFSE as Nb and Ta, with Rb, K, and Pb negative anomalies, similar to common patterns for OIB. These features are remarkably distinctive from MORB that exhibit depletion of both LILE and LREE. Therefore, the normal asthenospheric mantle cannot be the source region of these alkali basalts. Considering the postcollisional setting and the tectonic location of alkali basalts in the West Qinling orogen, the orogenic lithospheric mantle is the most likely site for their mantle source. The alkali basalts exhibit relatively depleted whole-rock Sr

explained by enrichment of K and Ti in hornblende or phlogopite [Foley *et al.*, 1996; Frost, 2006; Pilet *et al.*, 2008]. Compared to phlogopite, hornblende has much lower partition coefficients for Rb and Ba, but higher partition coefficient for Sr [LaTourrette *et al.*, 1995; Tiepolo *et al.*, 2007]. Partial melts from a hornblende-bearing mantle source should have lower Rb/Sr (<0.1) and higher Ba/Rb ratios (>20) than those from a phlogopite-bearing mantle source [Furman and Graham, 1999]. As presented in supporting information Table S2, the West Qinling alkali basalts generally have low Rb/Sr (0.002–0.0029) and high Ba/Rb (up to 171.5), suggesting the existence of hornblende in their mantle source. It has been suggested that hornblende veins in the suprasubduction-zone (SSZ) mantle wedge peridotite can serve as the source of some basaltic magmas in oceanic settings [e.g., Pilet *et al.*, 2011] and continental settings [e.g., Ma *et al.*, 2011, 2013; Jung *et al.*, 2012]. The hornblende veins can be generated by

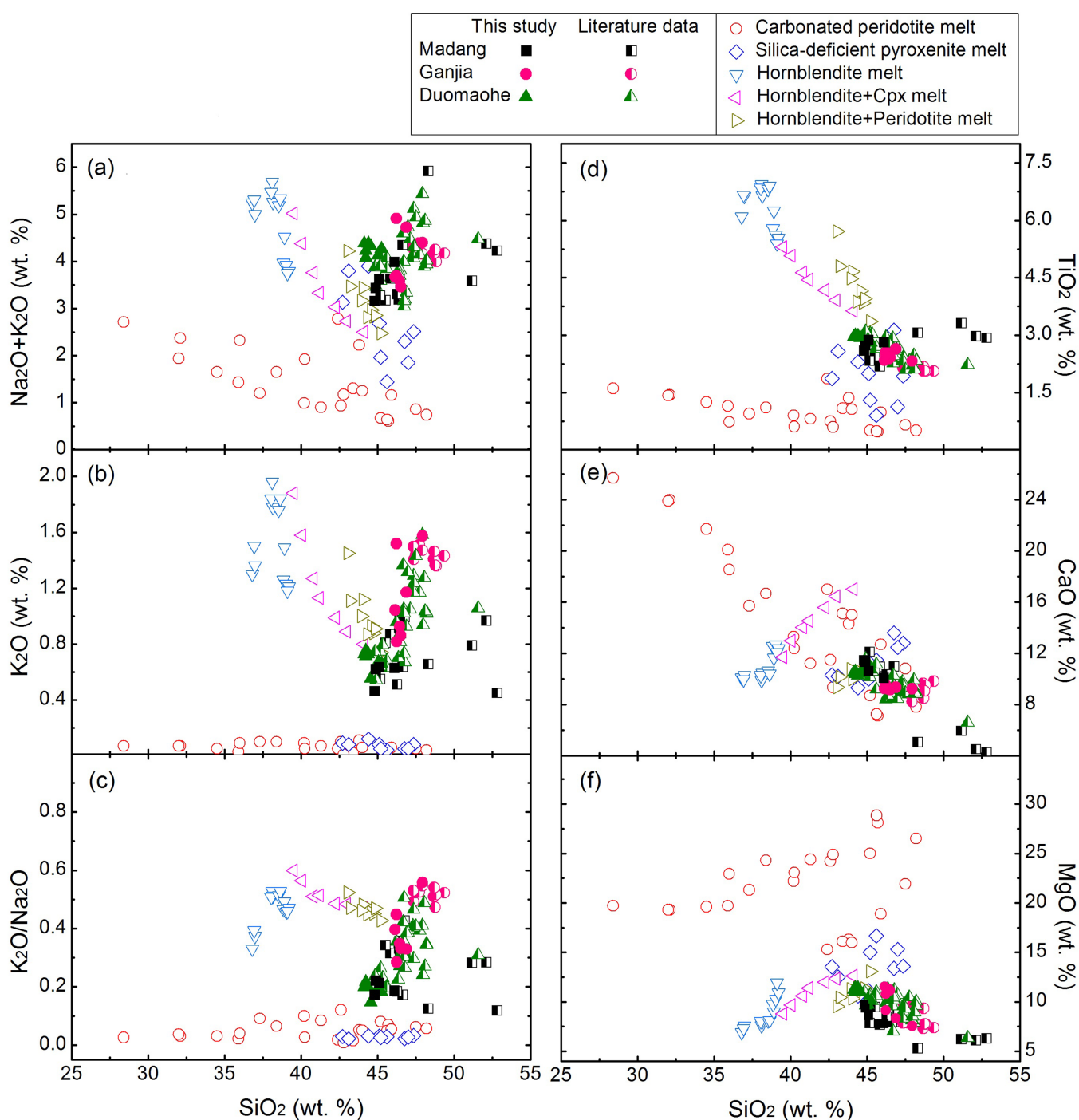


**Figure 7.** Plots of SiO<sub>2</sub> versus Na<sub>2</sub>O + K<sub>2</sub>O, K<sub>2</sub>O, K<sub>2</sub>O/Na<sub>2</sub>O, TiO<sub>2</sub>, CaO, and MgO for alkali basalts from West Qinling, showing that the hornblendite + peridotite sandwich most likely represents the mantle lithology in view of the available studies from experimental petrology. Data sources for the West Qinling alkali basalts: this study, Fan *et al.* [2007a, 2007b], Yan *et al.* [2012], Ding *et al.* [2013], and Li *et al.* [2013a]. Also shown are the experimental alkali melt compositions from different ultramafic lithologies, including carbonated peridotites [Hirose, 1997; Dasgupta *et al.*, 2007], silica-deficient pyroxenite [Hirschmann *et al.*, 2003; Kogiso *et al.*, 2003], and hornblendite, hornblendite + Cpx and hornblendite + peridotites [Pilet *et al.*, 2008].

Nd-Hf and zircon Hf isotope compositions (supporting information Tables S2 and S3), suggesting their derivation from a relatively deplete mantle source. They also have consistently young whole-rock Nd model ages of 136–625 Ma and whole-rock Hf model ages of 256–459 Ma (supporting information Table S2), suggesting their origination from the juvenile SCLM. Thus, the mantle source of alkali basalts from West Qinling would be the juvenile orogenic lithospheric mantle.

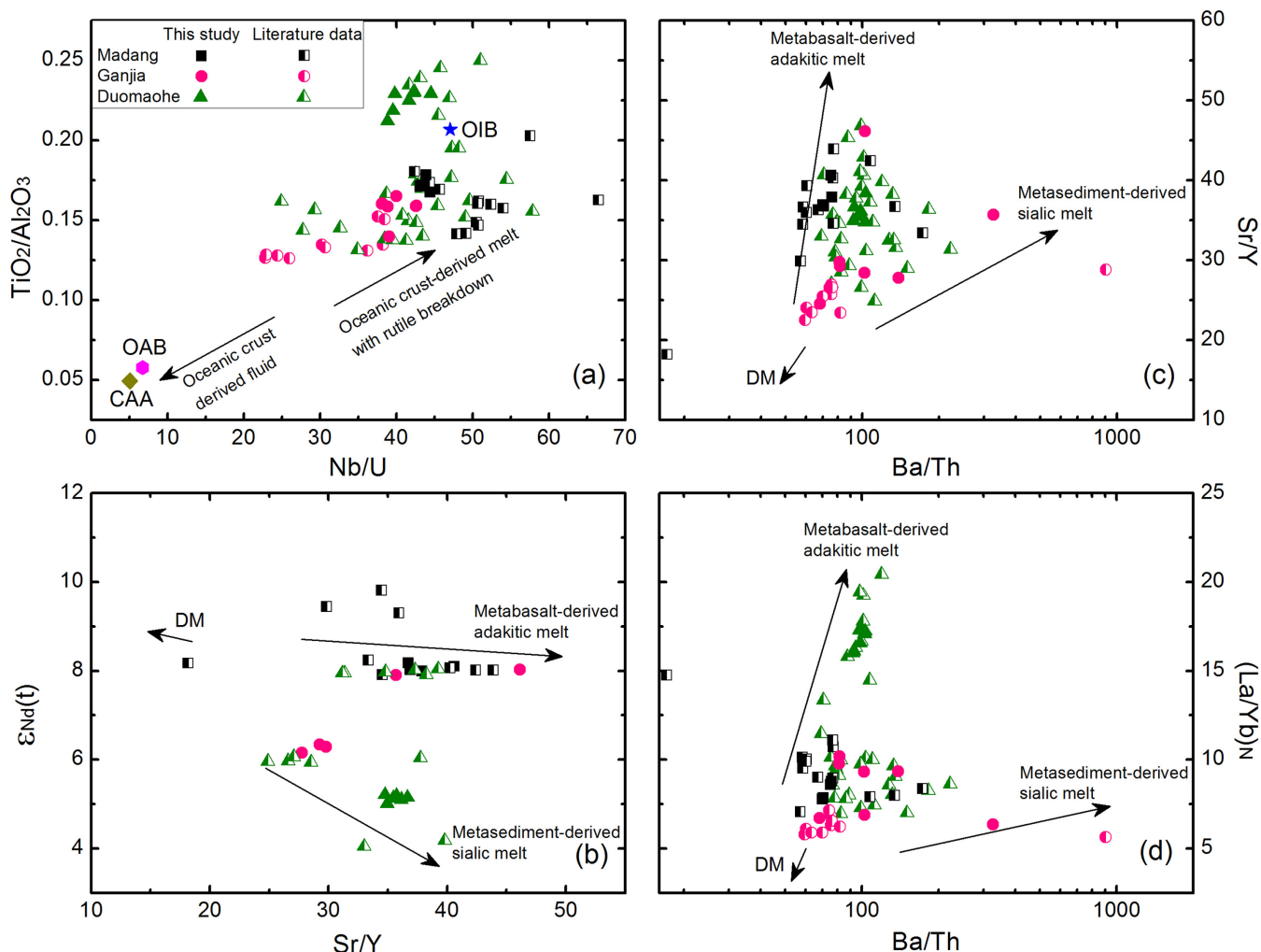


**Figure 8.** Plots of (a)  $\text{Nb}/\text{U}$  ratios versus  $\text{TiO}_2/\text{Al}_2\text{O}_3$ , (b)  $\varepsilon_{\text{Nd}}(\text{t})$  values versus  $\text{Sr/Y}$  ratios, (c)  $\text{Ba}/\text{Th}$  ratios versus  $\text{Sr/Y}$  ratios, and (d)  $\text{Ba}/\text{Th}$  ratios versus  $(\text{La}/\text{Yb})_N$  ratios for alkali basalts from West Qinling, showing the contribution of subducted oceanic crust-derived melts (including subducted oceanic metabasalt-derived adakitic melt and seafloor metasediment-derived sialic melt) with rutile breakdown to their mantle source. Data sources for the West Qinling alkali basalts: this study, Fan et al. [2007a, 2007b], Yan et al. [2012], Ding et al. [2013], and Li et al. [2013a]. Also shown are the oceanic island basalts (OIB) [Sun and McDonough, 1989], oceanic arc basalts (OAB) [Kelemen et al., 2003], and continental arc andesites (CAA) [Kelemen et al., 2003]. The depleted mantle peridotite (DM) composition is after Salters and Stracke [2004].

It has been suggested that deeply subducted oceanic crust would be partially melted at mantle depths of 120–300 km, leading to the breakdown of rutile [Ringwood, 1990; Zheng, 2012]. This can produce felsic melts not only with enrichment of LILE and LREE but also with enrichment or no depletion of such HFSE as Nb and Ta. These felsic melts would react with the overlying mantle wedge peridotite to generate the olivine-poor ultramafic lithologies such as pyroxenite and hornblendite, which could serve as the mantle sources for basaltic rocks with OIB-like trace element distribution patterns [e.g., Zhang et al., 2009; Xu et al., 2012]. As shown in Figure 8a, the contribution of rutile breakdown to the HFSE abundances of mantle sources is indicated by higher  $\text{TiO}_2/\text{Al}_2\text{O}_3$  and  $\text{Nb}/\text{U}$  ratios for the alkali basalts from West Qinling than common arc-like basalts. For oceanic arc basalts (OAB) and continental arc andesites (CAA), fluids released from subducting oceanic crust are depleted in Nb and Ta because of the dehydration in the rutile stability field. Thus, the OAB and CAA are characterized by the arc-like trace element distribution patterns, exhibiting low  $\text{Nb}/\text{U}$  and  $\text{TiO}_2/\text{Al}_2\text{O}_3$  ratios (Figure 8a). The Sr-Nd isotope compositions of alkali basalts also just lie between the depleted MORB mantle and Paleotethyan oceanic crust (Figure 5), suggesting a two-component mixing between the Paleotethyan oceanic crust and the isotopically depleted mantle. Along with their depleted Sr-Nd-Hf isotope compositions and the young Nd and Hf model ages, it is inferred that the alkali basalts from West Qinling would be derived from partial melting of the juvenile SCLM that was metasomatized by the felsic melts derived from deeply subducted oceanic crust.

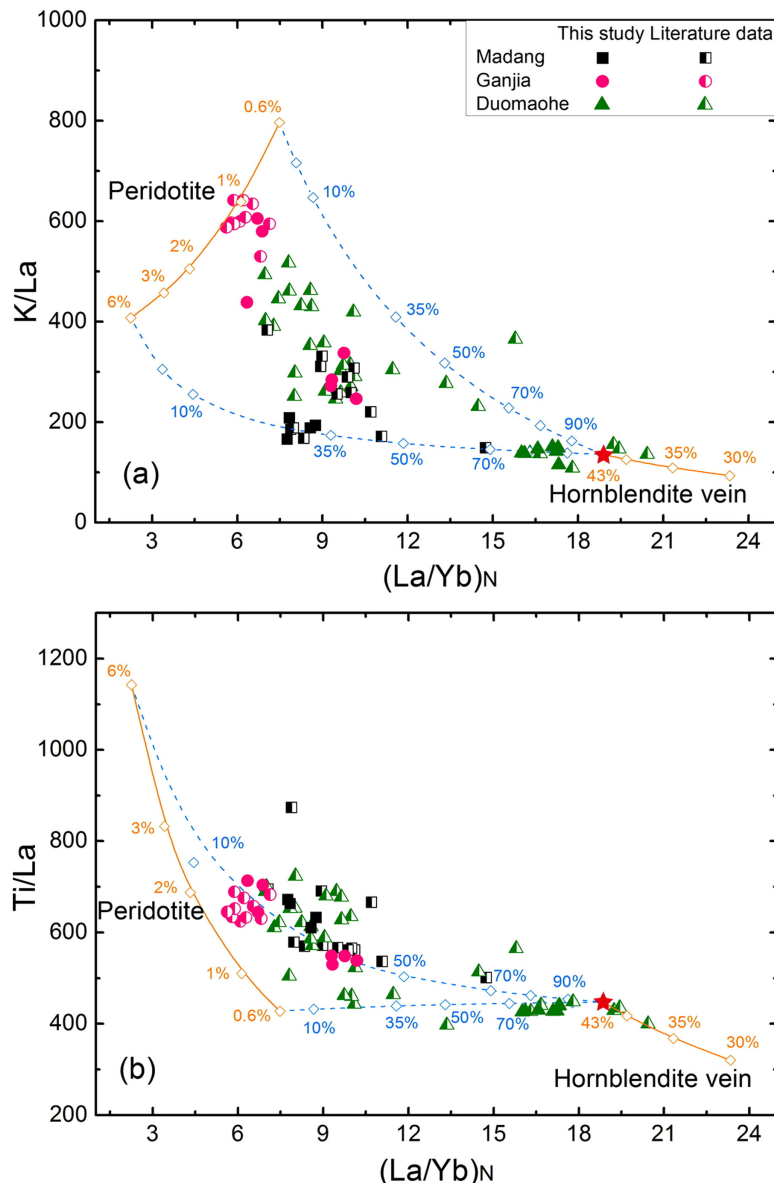


**Figure 9.** Plots of  $(\text{La/Yb})_N$  versus (a)  $\text{K/La}$  and (b)  $\text{Ti/La}$  ratios for Mesozoic alkali basalts from West Qinling, showing their derivation from partial melting of hornblendite vein plus peridotite in the orogenic lithospheric mantle. The continuous curves show nonmodal batch melting models for mantel peridotite and metasomatic hornblendite vein as starting materials, from 0.6 to 6% and from 30 to 43% melt fractions, respectively. The asterisk-finished hornblendite melting curve represents the complete consumption of amphibole (43% melt fractions), with  $\text{Ol} + \text{Cpx} + \text{Spl}$  as residual minerals. It should be noted that most of the alkali basalts plot between the peridotite and hornblendite melting curves calculated by the melting model. Data sources for the West Qinling alkali basalts: this study, Fan *et al.* [2007a, 2007b], Yan *et al.* [2012], Ding *et al.* [2013], and Li *et al.* [2013a]. The compositions of peridotite and hornblendite vein are after the primitive mantle [McDonough and Sun, 1995] and hornblendite AG4 [Pilet *et al.*, 2008], respectively. The parameters for melting models are listed in supporting information Table S4.

by partial melting of the subducted oceanic metabasalt with garnet as the residue. The third component is characterized by the lowest  $\varepsilon_{\text{Nd}}(\text{t})$  values but the highest  $\text{Ba/Th}$  ratios, corresponding to the sialic melt derived from partial melting of the subducted metasediment. Some of the alkali basalts exhibit positive  $\text{Pb}$  anomalies, also suggesting involvement of the metasediment-derived melt in their mantle source. Therefore, the both oceanic metabasalt-derived and metasediment-derived melts have contributed to the juvenile SCLM source of alkali basalts from West Qinling.

During the subduction of oceanic crust to mantle depths of  $>120$  km, high temperatures would be first acquired for its upper part composed of altered oceanic basalt and sea-floor sediment. Partial melting of the subducted metabasalt would generate the adakitic melt of high  $\text{Sr/Y}$  and  $(\text{La/Yb})_N$  ratios with garnet as a residual phase [Defant and Drummond, 1990], whereas partial melting of the metasediment yields the sialic melt of relatively low  $\text{Sr/Y}$  and  $(\text{La/Yb})_N$  ratios [Xu *et al.*, 2014]. On the other hand, the altered oceanic basalt commonly exhibits lower  $\text{Ba/Th}$  ratios but higher  $\varepsilon_{\text{Nd}}(\text{t})$  values than the terrestrial sediment [Plank and Langmuir, 1998; Kelley *et al.*, 2003; Straub *et al.*, 2010]. As illustrated in Figures 8b–8d, three-component mixing is evident in the diagrams of  $\text{Sr/Y}$  ratios versus  $\varepsilon_{\text{Nd}}(\text{t})$  values,  $\text{Ba/Th}$  ratios versus  $\text{Sr/Y}$  and  $(\text{La/Yb})_N$  ratios. The first component is the depleted mantle peridotite (DM), which is characterized by the highest  $\varepsilon_{\text{Nd}}(\text{t})$  values, low  $\text{Ba/Th}$ ,  $\text{Sr/Y}$ , and  $(\text{La}/\text{Yb})_N$  ratios. The second component is characterized by high  $\varepsilon_{\text{Nd}}(\text{t})$  values,  $\text{Sr/Y}$  and  $(\text{La/Yb})_N$  ratios, corresponding to the adakitic melt produced

The alkali basalts from West Qinling exhibit variable K/La and Ti/La ratios that are negatively correlated with  $(\text{La/Yb})_{\text{N}}$  ratios (Figure 9). They also display variable whole-rock  $\varepsilon_{\text{Nd}}(t)$  values of 4.0–9.8 (supporting information Table S2). The variable trace element and isotope compositions suggest that they cannot originate from a homogeneous mantle source. A two-component mixing trend is well defined on the diagrams of whole-rock  $(\text{La/Yb})_{\text{N}}$  ratios vs. K/La and Ti/La ratios (Figure 9). One is the metasomatic hornblendite as inferred in section 5.1, and the other is the mantle wedge peridotite. Peridotite-derived melts generally have low  $(\text{La/Yb})_{\text{N}}$ , K/La, and Ti/La ratios relative to those from hornblendite [Haase *et al.*, 2004; Ma *et al.*, 2011; Jung *et al.*, 2012]. The parameters for calculation of partial melting are presented in supporting information Table S4. The compositions of peridotite and hornblendite are those of the primitive mantle peridotite [McDonough and Sun, 1995] and hornblendite AG4 [Pilet *et al.*, 2008], respectively. Since the alkali basalts used in this study exhibit insignificant fractionation between MREE and HREE (Figure 4a), spinel peridotite was used in the melting modeling.

As shown in Figure 9, the asterisk-finished hornblendite melting curve is calculated by complete consumption of amphibole, with OI + Cpx + Spl as residual minerals. Since hornblendite is more susceptible to partial melting than peridotite, partial melting of the peridotite would occur after the complete consumption of amphibole in the mantle sources. Most of the alkali basalts plot between the peridotite and hornblendite melting curves calculated by the melting model. They can be interpreted as the products of varying degrees of mixing between hornblendite-derived and peridotite-derived melts, with minor contributions from peridotite melting (~0.6–6% melt fractions). According to this melting model, there are high contributions from hornblendite-derived melts to the mantle source for the Duomahe alkali basalts that exhibit high  $(\text{La/Yb})_{\text{N}}$  ratios, low K/La and Ti/La ratios. In contrast, there are low contributions from hornblendite-derived melts to the mantle source for the Madang and Ganjia basalts that exhibit relatively low  $(\text{La/Yb})_{\text{N}}$  ratios, high K/La and Ti/La ratios. In addition, the Duomahe alkali basalts generally display lower whole-rock  $\varepsilon_{\text{Nd}}(t)$  values than those of Madang and Ganjia basalts (Figure 8b), which is consistent with the composition of metasomatic hornblendite in that the subducted crustal rocks would display lower  $\varepsilon_{\text{Nd}}(t)$  values than the mantle peridotite. This melting model is also consistent with the outcome of experimental petrology that partial melting of peridotite alone cannot produce alkali basalts. The addition of metasomatic hornblendite to the mantle source is substantial to the generation of alkali basalts from West Qinling. Therefore, the both major-trace element and radiogenic isotope features of alkali basalts can be explained by the hornblendite vein + peridotite sandwich melting model. A similar model has also been suggested for the petrogenesis of K-rich mafic dykes and continental intraplate basalts [e.g., Yang *et al.*, 2004; Ma *et al.*, 2011].

## 6. Implications for Recycling of Paleotethyan Oceanic Crust in Collisional Orogen

It has been suggested that the Qinling orogen was finally formed with the continental collision between the South Qinling and the South China Block in the Triassic subsequent to the closure of A'nimaque-Mianlue Paleotethyan sea in the Late Paleozoic [Meng and Zhang, 2000; Meng *et al.*, 2005; Dong *et al.*, 2011; Wu and Zheng, 2013]. The subducted Paleotethyan oceanic crust would be partially melting at mantle depths of >120 km during this tectonism. As discussed above, this can produce felsic melts with enrichment of LILE and LREE but no depletion of Nb and Ta due to the breakdown of rutile [Ringwood, 1990; Zheng, 2012]. Such felsic melts would react with the overlying juvenile SCLM peridotite to generate the mantle source of alkali basalts from West Qinling. The contribution of rutile breakdown to the mantle sources of intraplate basalts is confirmed by the high  $\text{TiO}_2/\text{Al}_2\text{O}_3$  and Nb/U ratios than common arc-like basalts (Figure 8a).

In view of the above arguments, petrogenesis of the alkali basalts from West Qinling also can be outlined by the SARSH model of Zhao *et al.* [2013] in the following five steps. (1) Subduction (S): the fossil oceanic crust was subducted beneath the SCLM to depths of >120 km. (2) Anatexis (A): anatexis of the subducted oceanic crust, producing felsic melts that are enriched in LILE and LREE but no depletion of Nb and Ta due to the breakdown of rutile. (3) Reaction (R): the felsic melts would react with the overlying SCLM wedge peridotite, generating the fertile mantle metasomes in ultramafic lithologies such as hornblendite and pyroxenite. (4) Storage (S): the fertile metasomes would be stored in the orogenic lithospheric mantle for over one hundred of million years. (5) Heating (H): the metasomes would become partially melted together their host peridotite due to heating at the base of the collisional orogen, giving rise to the basaltic melts with OIB-like trace element distribution patterns. For the West Qinling alkali basalts, the hornblendite would be generated by the reaction of Paleotethyan oceanic crust-derived melts with the overlying juvenile SCLM

peridotite in the oceanic subduction channel during the subduction of Late Paleozoic. These alkali basalts mainly erupted in the Early Cretaceous, remarkably later than the Triassic continental collision. With respect to the tectonic mechanism for the alkali magmatism of Early Cretaceous, it may be ascribed to decompression melting of the fertile mantle domains (hornblendite + peridotite sandwich) due to lithospheric extension in the postcollisional stage. This is consistent with the common idea whether and when tectonic collapse and associated magmatism occur in orogenic belts are controlled by local or regional geodynamic processes [Dilek and Altunkaynak, 2007]. We suggest that the metasomatic hornblendite veins may be common in the SSZ lithospheric mantle that would be generated by the melt-peridotite reaction at the slab-mantle interface in the oceanic subduction channel. The crustal metasomatism at the base of the mantle wedge is the key to the formation of mantle sources for continental alkali basalts.

Therefore, the recycling of Paleotethyan oceanic crust into the mantle of Paleozoic age is realized by the melt-peridotite at the slab-mantle interaction in the Paleotethyan oceanic subduction channel. The dehydration melting of subducting crustal rocks and subsequent melt-peridotite reaction are two key processes to generate the ultramafic metasomes in the suprasubduction-channel (SSC) mantle wedge. Similar tectonic processes would have also operated in modern oceanic subduction zones, where dehydration of the subducting oceanic crust and subsequent fluid-peridotite reaction generate fertile and hydrous mantle sources for common arc basalts [Kelemen et al., 1993, 2003; Schmidt and Poli, 2003]. Likewise, dehydration melting of the subducting continental crust and subsequent melt-peridotite reaction generate fertile and enriched orogenic SCLM sources for postcollisional mafic igneous rocks [Zhao et al., 2013]. Therefore, the property of metasomatic agents attending the chemical reaction at the slab-mantle interface in oceanic and continental subduction channels is substantial to the type of SSC mafic magmatism.

## 7. Conclusions

The Mesozoic alkali basalts from the West Qinling orogen mainly erupted at 101–112 Ma, remarkably later than the Triassic continental collision. They exhibit significant enrichment of melt-mobile incompatible trace elements such as LILE and LREE, and no depletion of melt-immobile incompatible trace elements such as Nb and Ta. This is similar to the common OIB but significantly different from normal MORB, suggesting their origination from fertile SCLM. In addition, they display relative depletion of radiogenic isotope compositions with young whole-rock Hf and Nd model ages, indicating their origination from juvenile SCLM. The Late Paleozoic subduction of the Paleotethyan oceanic crust and subsequent slab-mantle interaction are suggested as a possible tectonic mechanism for the formation of such a fertile mantle source. The reaction of the juvenile SCLM wedge peridotite with felsic melts derived from the subducting oceanic crust would generate the fertile mantle metasomes with ultramafic lithology such as hornblendite. Partial melting of the hornblendite + peridotite sandwich can account for the petrological and geochemical features observed from the alkali basalts. Therefore, the metasomatic hornblendite veins may be common in the SSC lithospheric mantle, and they can serve as the mantle source of SSC alkali basalts. The orogenic alkali basalts not only provide valuable information about the lithology of local SCLM domains above fossil subduction channels, but also record the recycling of subducted fossil oceanic crust.

### Acknowledgments

Data supporting Figures 2–9 are available in supporting information Tables S1–S4. This study was supported by grants from the Natural Science Foundation of China (41125012, 41221062) and by the Fundamental Funds for the Central Universities (WK2080000032, WK2080000054). Thanks are due to Yongsheng Liu for his assistance with whole-rock trace element analyses and LA-ICPMS zircon U-Pb dating, to Fu-Qiang Dai, Yueheng Yang, and Jinhui Yang for their assistance with whole-rock radiogenic isotope and LA-MC-ICPMS zircon Lu-Hf isotope analyses. We are grateful to C.-T. A. Lee and an anonymous reviewer for their comments that greatly helped in the improvement of the presentation.

## References

- Balcaen, L., I. D. Schrijver, L. Moens, and F. Vanhaecke (2005), Determination of the  $^{87}\text{Sr}/^{86}\text{Sr}$  isotope ratio in USGS silicate reference materials by multi-collector ICP-mass spectrometry, *Int. J. Mass Spectrom.*, 242, 251–255.
- Blichert-Toft, J., and F. Albarède (1997), The Lu-Hf isotope geochemistry of chondrites and the evolution of the mantle-crust system, *Earth Planet. Sci. Lett.*, 148, 243–258.
- Coltorti, M., C. Bonadiman, B. Faccini, M. Grégoire, S. Y. O'Reilly, and W. Powell (2007), Amphiboles from suprasubduction and intraplate lithospheric mantle, *Lithos*, 99, 68–84.
- Dasgupta, R., M. M. Hirschmann, and N. D. Smith (2007), Partial melting experiments of peridotite + CO<sub>2</sub> at 3 GPa and genesis of alkalic ocean island basalts, *J. Petrol.*, 48, 2093–2124.
- Defant, M. J., and M. S. Drummond (1990), Derivation of some modern arc magmas by melting of young subducted lithosphere, *Nature*, 347, 662–665.
- Dilek, Y., and S. Altunkaynak (2007), Cenozoic crustal evolution and mantle dynamics of postcollisional magmatism in western Anatolia, *Int. Geol. Rev.*, 49, 431–453.
- Ding, Y., X.-H. Yu, X.-X. Mo, X.-W. Li, X.-F. Huang, and P. Wei (2013), Geochronology, geochemistry and petrogenesis of the Hongqiang basalts from Northeast Qinghai-Tibetan Plateau, *Earth Sci. Front.*, 20, 180–191.
- Dong, Y., G. Zhang, F. Neubauer, X. Liu, J. Genser, and C. Hauzenberger (2011), Tectonic evolution of the Qinling orogen, China: Review and synthesis, *J. Asian Earth Sci.*, 41, 213–237.

- Downes, H. (2007), Origin and significance of spinel and garnet pyroxenites in the shallow lithospheric mantle: Ultramafic massifs in orogenic belts in Western Europe and NW Africa, *Lithos*, 99, 1–24.
- Downes, H., A. Beard, and R. Hinton (2004), Natural experimental charges: An ion-microprobe study of trace element distribution coefficients in glass-rich hornblende and clinopyroxenite xenoliths, *Lithos*, 75, 1–17.
- Elhlou, S., E. Belousova, W. L. Griffin, N. J. Pearson, and S. Y. O'Reilly (2006), Trace element and isotopic composition of GJ red zircon standard by laser ablation, *Geochim. Cosmochim. Acta*, 70, A158, doi:10.1016/j.gca.2006.06.1383.
- Fan, L. Y., Y. J. Wang, X. Y. Li, and C. W. Li (2007a), Geochemical characteristics of late mesozoic mafic volcanic rocks from Western Qinling and its tectonic implications, *Geotect. Metallogen.*, 31, 471–481.
- Fan, L. Y., Y. J. Wang, and X. Y. Li (2007b), Geochemical characteristics of late mesozoic mafic volcanic rocks from Western Qinling and its tectonic implications, *J. Mineral. Petrol. Econ. Geol.*, 27, 63–72.
- Feng, Y., X. Cao, E. Zhang, Y. Hu, X. Pan, J. Yang, Q. Jia, and W. Li, (2002), *Structure, Orogenic Processes and Geodynamic of the Western Qinling Orogen*, 263 pp., Xi'an Map Press, Xi'an, China.
- Foley, S. F., S. E. Jackson, J. D. Fryer, and G. A. J. Greenough (1996), Trace element partition coefficients for clinopyroxene and phlogopite in an alkaline lamprophyre from Newfoundland by LAM-ICP-MS, *Geochim. Cosmochim. Acta*, 60, 629–638.
- Frost, D. J. (2006), The stability of hydrous mantle phases, *Rev. Mineral. Geochem.*, 62, 243–271.
- Fu, B., Y. F. Zheng, and J. L. R. Touret (2002), Petrological, isotopic and fluid inclusion studies of eclogites from Sujahe, NW Dabie Shan (China), *Chem. Geol.*, 187, 107–128.
- Furman, T., and D. Graham (1999), Erosion of lithospheric mantle beneath the East African Rift system: Geochemical evidence from the Kivu volcanic province, *Lithos*, 48, 237–262.
- Griffin, W. L., N. J. Pearson, E. Belousova, S. E. Jackson, E. van Achterbergh, S. Y. O'Reilly, and S. R. Shee (2000), The Hf isotope composition of cratonic mantle: LA-MC-ICPMS analysis of zircon megacrysts in kimberlites, *Geochim. Cosmochim. Acta*, 64, 133–147.
- Haase, K. M., B. Goldschmidt, and D. Garbe-Schonberg (2004), Petrogenesis of Tertiary continental intra-plate lavas from the Westerwald region, Germany, *J. Petrol.*, 45, 883–905.
- Hacker, B. R., L. Ratschbacher, and J. G. Liou (2004), Subduction, collision, and exhumation in the Qinling-Dabie Orogen, *J. Geol. Soc. London*, 226, 157–175.
- Herzberg, C. (2011), Identification of source lithology in the Hawaiian and Canary islands: Implications for origins, *J. Petrol.*, 52, 113–146.
- Hirose, K. (1997), Partial melt compositions of carbonated peridotite at 3 GPa and role of CO<sub>2</sub> in alkali-basalt magma generation, *Geophys. Res. Lett.*, 24, 2837–2840.
- Hirose, K., and I. Kushiro (1993), Partial melting of dry peridotites at high pressures: Determination of compositions of melts segregated from peridotite using aggregates of diamond, *Earth Planet. Sci. Lett.*, 114, 477–489.
- Hirschmann, M. M., T. Kogiso, M. B. Baker, and E. M. Stolper (2003), Alkalic magmas generated by partial melting of garnet pyroxenite, *Geology*, 31, 481–484.
- Hofmann, A. W. (1997), Mantle geochemistry: The message from oceanic volcanism, *Nature*, 385, 219–229.
- Iizuka, T., and T. Hirata (2005), Improvements of precision and accuracy in in situ Hf isotope microanalysis of zircon using the laser ablation-MC-ICPMS technique, *Chem. Geol.*, 220, 121–137.
- Ito, E., W. M. White, and C. Gopel (1987), The O, Sr, Nd and Pb isotope geochemistry of MORB, *Chem. Geol.*, 62, 157–176.
- Jung, S., K. Vieten, R. L. Romer, K. Mezger, S. Hoernes, and M. Satir (2012), Petrogenesis of tertiary alkaline magmas in the Siebengebirge, Germany, *J. Petrol.*, 53, 2381–2409.
- Kelemen, P. B., N. Shimizu, and T. Dunn (1993), Relative depletion of niobium in some arc magmas and the continental crust: Partitioning of K, Nb, La and Ce during melt/rock reaction in the upper mantle, *Earth Planet. Sci. Lett.*, 120, 111–134.
- Kelemen, P. B., K. Hanghoj, and A. R. Greene (2003), One view of the geochemistry of subduction-related magmatic arcs, with an emphasis on primitive andesite and lower crust, in *The Crust*, edited by R. L. Rudnick, pp. 593–659, Elsevier, N. Y.
- Kelley, K. A., T. Plank, J. Ludden, and H. Staudigel (2003), Composition of altered oceanic crust at ODP Sites 801 and 1149, *Geochim. Geophys. Geosyst.*, 4(6), 8910, doi:10.1029/2002GC000435.
- Keshav, S., G. H. Gudfinnsson, G. Sen, and Y. Fei (2004), High-pressure melting experiments on garnet clinopyroxenite and the alkalic to tholeiitic transition in ocean-island basalts, *Earth Planet. Sci. Lett.*, 223, 365–379.
- Kogiso, T., M. M. Hirschmann, and D. J. Frost (2003), High-pressure partial melting of garnet pyroxenite: Possible mafic lithologies in the source of ocean island basalts, *Earth Planet. Sci. Lett.*, 216, 603–617.
- Kogiso, T., M. M. Hirschmann, and M. Pertermann (2004), High-pressure partial melting of mafic lithologies in the mantle, *J. Petrol.*, 45, 2407–2422.
- Kushiro, I. (1996), Partial melting of a fertile mantle peridotite at high pressures: An experimental study using aggregates of diamond, in *Earth Processes: Reading the Isotopic Code*, *Geophys. Monogr.*, vol. 95, edited by A. Basu and S. Hart, pp. 109–122, AGU, Washington, D. C.
- LaTourrette, T., R. L. Hervig, and J. R. Holloway (1995), Trace element partitioning between amphibole, phlogopite, and basanite melt, *Earth Planet. Sci. Lett.*, 135, 13–30.
- Le Bas, M. J., R. W. Le Maître, A. Streckeisen, and B. Zanettin (1986), A chemical classification of volcanic rocks based on the total alkali-silica diagram, *J. Petrol.*, 27, 745–750.
- Le Roux, V., C. T. A. Lee, and S. J. Turner (2010), Zn/Fe systematics in mafic and ultramafic systems: Implications for detecting major element heterogeneities in the Earth's mantle, *Geochim. Cosmochim. Acta*, 74, 2779–2796.
- Le Roux, V., R. Dasgupta, and C. T. A. Lee (2011), Mineralogical heterogeneities in the Earth's mantle: Constraints from Mn, Co, Ni and Zn partitioning during partial melting, *Earth Planet. Sci. Lett.*, 307, 395–408.
- Lee, C.-T. A., P. Luffi, V. Le Roux, R. Dasgupta, F. Albaréde, and W. P. Leeman (2010), The redox state of arc mantle using Zn/Fe systematics, *Nature*, 468, 681–685.
- Li, S. G., Y. Chen, B. L. Cong, Z. Zhang, R. Zhang, D. Liou, S. R. Hart, and N. Ge (1993), Collision of the North China and Yangtze blocks and formation of coesite-bearing eclogites: Timing and processes, *Chem. Geol.*, 109, 70–89.
- Li, X.-W., X.-X. Mo, X.-H. Yu, Y. Ding, X.-F. Huang, P. Wei, and W.-Y. He (2013a), Geochronological, geochemical and Sr-Nd-Hf isotopic constraints on the origin of the Cretaceous intraplate volcanism in West Qinling, Central China: Implications for asthenosphere-lithosphere interaction, *Lithos*, 177, 381–401.
- Li, X.-W., X.-X. Mo, X.-H. Yu, Y. Ding, X.-F. Huang, P. Wei, and W.-Y. He (2013b), Petrology and geochemistry of the early Mesozoic pyroxene andesites in the Maixiu Area, West Qinling, China: Products of subduction or syn-collision?, *Lithos*, 172–173, 158–174.
- Liu, Y. S., K. Q. Zong, P. B. Kelemen, and S. Gao (2008a), Geochemistry and magmatic history of eclogites and ultramafic rocks from the Chinese continental scientific drill hole: Subduction and ultrahigh-pressure metamorphism of lower crustal cumulates, *Chem. Geol.*, 247, 133–153.

- Liu, Y. S., Z. C. Hu, S. Gao, D. Günther, J. Xu, C. G. Gao, and H. H. Chen (2008b), In situ analysis of major and trace elements of anhydrous minerals by LA-ICP-MS without applying an internal standard, *Chem. Geol.*, 257, 34–43.
- Liu, Y. S., S. Gao, Z. C. Hu, C. Gao, K. Zong, and D. Wang (2010), Continental and oceanic crust recycling-induced melt-peridotite interactions in the Trans-North China Orogen: U-Pb dating, Hf isotopes and trace elements in zircons from mantle xenoliths, *J. Petrol.*, 51, 537–571.
- Lu, X. X. (1999), *Tectonic Map of Granitoids in Qinling*, Xi'an Geol. Publ. House, Xi'an, China.
- Ludwig, K. R. (2003), *ISOPLOT 3.00: A Geochronological Toolkit for Microsoft Excel*, Berkeley Geochronol. Center, Berkeley, Calif.
- Ma, G. S.-K., J. Malpas, C. Xenophontos, and G. H.-N. Chan (2011), Petrogenesis of latest Miocene-Quaternary continental intraplate volcanism along the northern Dead Sea Fault System (Al Ghab-Homs Volcanic Field), western Syria: Evidence for lithosphere-asthenosphere interaction, *J. Petrol.*, 52, 401–430.
- Ma, G. S. K., J. Malpas, K. Suzuki, C.-H. Lo, K.-L. Wang, Y. Iizuka, and C. Xenophontos (2013), Evolution and origin of the Miocene intraplate basalts on the Aleppo Plateau, NW Syria, *Chem. Geol.*, 335, 149–171.
- Malaspina, N., J. Hermann, M. Scambelluri, and R. Compagnoni (2006), Polyphase inclusions in garnet-orthopyroxenite (Dabie Shan, China) as monitors for metasomatism and fluid-related trace element transfer in subduction zone peridotite, *Earth Planet. Sci. Lett.*, 249, 173–187.
- McDonough, W. F., and S. S. Sun (1995), The composition of the Earth, *Chem. Geol.*, 120, 223–253.
- Meng, Q. R., and G. W. Zhang (1999), Timing of collision of the North and South China blocks: Controversy and reconciliation, *Geology*, 27, 1–96.
- Meng, Q. R., and G. W. Zhang (2000), Geologic framework and tectonic evolution of the Qinling orogen, Central China, *Tectonophysics*, 323(3–4), 183–196.
- Meng, Q.-R., E. Wang, and J.-M. Hu (2005), Mesozoic sedimentary evolution of the northwest Sichuan basin: Implication for continued clockwise rotation of the South China block, *Geol. Soc. Am. Bull.*, 117, 396–410.
- Münker, C., S. Weyer, E. Scherer, and K. Mezger (2001), Separation of high field strength elements (Nb, Ta, Zr, Hf) and Lu from rock samples for MC-ICPMS measurements, *Geochem. Geophys. Geosyst.*, 2, 1064–1083.
- Niu, Y. (2008), The origin of alkaline lavas, *Science*, 320, 883–884.
- Niu, Y., and M. J. O'Hara (2003), Origin of ocean island basalts: A new perspective from petrology, geochemistry, and mineral physics considerations, *J. Geophys. Res.*, 108(B4), 2209, doi:10.1029/2002JB002048.
- Niu, Y., M. Wilson, E. R. Humphreys, and M. J. O'Hara (2011), The origin of intra-plate ocean island basalts (OIB): The lid effect and its geodynamic implications, *J. Petrol.*, 52, 1443–1468.
- Pertermann, M., and M. M. Hirschmann (2003), Partial melting experiments on a MORB-like pyroxenite between 2 and 3 GPa; constraints on the presence of pyroxenite in basalt source regions from solidus location and melting rate, *J. Geophys. Res.*, 108(B2), 2125, doi: 10.1029/2000JB000118.
- Pilet, S., M. B. Baker, and E. M. Stolper (2008), Metasomatized lithosphere and the origin of alkaline lavas, *Science*, 320, 916–919.
- Pilet, S., M. B. Baker, O. Muntener, and E. M. Stolper (2011), Monte Carlo simulations of metasomatic enrichment in the lithosphere and implications for the source of alkaline basalts, *J. Petrol.*, 52, 1415–1442.
- Plank, T., and C. H. Langmuir (1998), The chemical composition of subducting sediment and its consequences for the crust and mantle, *Chem. Geol.*, 145, 323–394.
- Powell, W., M. Zhang, S. Y. O'Reilly, and M. Tiepolo (2004), Mantle amphibole trace-element and isotopic signatures trace multiple metasomatic episodes in lithospheric mantle, western Victoria, Australia, *Lithos*, 75, 141–171.
- Prouteau, G., B. Scaillet, M. Pichavant, and R. Maury (2001), Evidence for mantle metasomatism by hydrous silicic melts derived from subducted oceanic crust, *Nature*, 410, 197–200.
- Prytulak, J., and T. Elliott (2007), TiO<sub>2</sub> enrichment in ocean island basalts, *Earth Planet. Sci. Lett.*, 263, 388–403.
- Qin, J. F., S. C. Lai, and Y. J. Li (2008), Slab breakoff model for the Triassic post-collisional adakitic granitoids in the Qinling orogen, central China: Zircon U-Pb ages, geochemistry, and Sr-Nd-Pb isotopic constraints, *Int. Geol. Rev.*, 50, 1080–1104, doi:10.2747/0020-6814.50.12.1080.
- Qin, J. F., S. C. Lai, G. Rodney, C. R. Diwu, Y. J. Ju, and Y. F. Li (2009), Geochemical evidence for origin of magma mixing for the Triassic monzonitic granite and its enclaves at Mishulung in the Qinling orogen (central China), *Lithos*, 112, 259–276.
- Rapp, R. P., N. Shimizu, M. D. Norman, and G. S. Applegate (1999), Reaction between slab-derived melts and peridotite in the mantle wedge: Experimental constraints at 3.8 GPa, *Chem. Geol.*, 160, 335–356.
- Rapp, R. P., M. D. Norman, D. Laporte, G. M. Yaxley, H. Martin, and S. F. Foley (2010), Continent formation in the Archean and chemical evolution of the cratonic lithosphere: Melt-rock reaction experiments at 3–4 GPa and petrogenesis of Archean Mg-diorites (Sanukitoids), *J. Petrol.*, 51, 1237–1266.
- Ringwood, A. E. (1990), Slab-mantle interactions. 3: Petrogenesis of intraplate magmas and structure of the upper mantle, *Chem. Geol.*, 82, 187–207.
- Salters, V. J. M., and A. Stracke (2004), Composition of the depleted mantle, *Geochem. Geophys. Geosyst.*, 5, Q05004, doi:10.1029/2003GC000597.
- Scherer, E., C. Munker, and K. Mezger (2001), Calibration of the lutetium-hafnium clock, *Science*, 293, 683–687.
- Schmidt, M. W., and S. Poli (2003), Generation of mobile components during subduction of oceanic crust, *Treat. Geochem.*, 3, 567–591.
- Sobolev, A. V., A. W. Hofmann, S. V. Sobolev, and I. K. Nikogosian (2005), An olivine-free mantle source of Hawaiian shield basalts, *Nature*, 434, 590–597.
- Sobolev, S. V., A. V. Sobolev, D. V. Kuzmin, N. A. Krivolutskaya, A. G. Petrunin, N. T. Arndt, V. A. Radko, and Y. R. Vasilev (2011), Linking mantle plumes, large igneous provinces and environmental catastrophes, *Nature*, 477, 312–316.
- Stracke, A. (2012), Earth's heterogeneous mantle: A product of convection-driven interaction between crust and mantle, *Chem. Geol.*, 330–331, 274–299.
- Straub, S. M., S. L. Goldstein, C. Class, A. Schmidt, and A. Gomez-Tuena (2010), Slab and mantle controls on the Sr-Nd-Pb-Hf isotope evolution of the post 42 Ma Izu-Bonin volcanic arc, *J. Petrol.*, 51, 993–1026.
- Sun, S.-s., and W. F. McDonough (1989), Chemical and isotopic systematics of oceanic basalts: Implications for mantle composition and processes, *Geol. Soc. Spec. Publ.*, 42, 313–345.
- Takahashi, E., and I. Kushiro (1983), Melting of a dry peridotite at high pressures and basalt magma genesis, *Am. Mineral.*, 68, 859–879.
- Tiepolo, M., R. Oberti, A. Zanetti, R. Vannucci, and S. F. Foley (2007), Trace-element partitioning between amphibole and silicate melt, *Rev. Mineral. Geochem.*, 67, 417–452.
- Walter, M. J. (1998), Melting of garnet peridotite and the origin of komatiite and depleted lithosphere, *J. Petrol.*, 39, 29–60.

- Wang, T., P. Ni, W. Sun, K. Zhao, and X. Wang (2011a), Zircon U-Pb ages of granites at Changba and Huangzhuguan in western Qinling and implications for source nature, *Chin. Sci. Bull.*, 56, 659–669.
- Wang, X. X., T. Wang, B. M. Jahn, N. G. Hu, and W. Chen (2007), Tectonic significance of Late Triassic post-collisional lamprophyre dykes from the Qinling Mountains (China): 40Ar-39Ar dating, trace element and Sr-Nd, isotope characteristics, *Geol. Mag.*, 144(4), 1–12.
- Wang, X. X., T. Wang, Q. J. Qi, and S. Li (2011b), Temporal and spatial variations, origin evolution and their tectonic significance of the Late Mesozoic granites in Qinling, central China, *Acta Petrol. Sin.*, 27(6), 1573–1593.
- Wang, X. X., T. Wang, and C. Zhang, (2013), Neoproterozoic, Paleozoic, and Mesozoic granitoid magmatism in the Qinling Orogen, China: Constraints on orogenic process, *J. Asian Earth Sci.*, 72, 129–151.
- Wasylenski, L. E., M. B. Baker, A. J. R. Kent, and E. M. Stolper (2003), Near-solidus melting of the shallow upper mantle: Partial melting experiments on depleted peridotite, *J. Petrol.*, 44, 1163–1191.
- Weis, D., et al. (2006), High-precision isotopic characterization of USGS reference materials by TIMS and MC-ICP-MS, *Geochem. Geophys. Geosyst.*, 7, Q08006, doi:10.1029/2006GC001283.
- Weis, D., B. Kieffer, D. Hanano, I. Nobre Silva, J. Barling, W. Pretorius, C. Maerschalk, and N. Mattielli (2007), Hf isotope compositions of U.S. Geological Survey reference materials, *Geochem. Geophys. Geosyst.*, 8, Q06006, doi:10.1029/2006GC001473.
- Wiedenbeck, M., P. Alle, F. Corfu, W. L. Griffin, M. Meier, F. Oberli, A. V. Quadt, J. C. Roddick, and W. Spiegel (1995), Three natural zircon standards for U-Th-Pb, Lu-Hf, trace element and REE analyses, *Geostand. Geoanal. Res.*, 19, 1–23.
- Woodhead, J. D., and J. M. Hergt (2005), Preliminary appraisal of seven natural zircon reference materials for in situ Hf isotope determination, *Geostand. Geoanal. Res.*, 29, 183–195.
- Wu, F.-Y., Y.-H. Yang, L.-W. Xie, J.-H. Yang, and P. Xu (2006), Hf isotopic compositions of the standard zircons and baddeleyites used in U-Pb geochronology, *Chem. Geol.*, 234, 105–126.
- Wu, Y.-B., and Y.-F. Zheng (2013), Tectonic evolution of a composite collision orogen: An overview on the Qinling-Tongbai-Hong'an-Dabie-Sulu orogen belt in central China, *Gondwana Res.*, 23, 1402–1428.
- Xu, P., F. Y. Wu, L. W. Xie, and Y. H. Yang (2004), Hf isotopic compositions of the standard zircons for U-Pb dating, *Chin. Sci. Bull.*, 49, 1642–1648.
- Xu, Z., Z.-F. Zhao, and Y.-F. Zheng (2012), Slab-mantle interaction for thinning of cratonic lithospheric mantle in North China: Geochemical evidence from Cenozoic continental basalts in central Shandong, *Lithos*, 146–147, 202–217.
- Xu, Z., Y.-F. Zheng, H.-Y. He, and Z.-F. Zhao (2014), Phenocryst He-Ar isotopic and whole-rock geochemical constraints on the origin of crustal components in the mantle source of Cenozoic continental basalt in eastern China, *J. Volcanol. Geotherm. Res.*, 272, 99–110.
- Yan, Z., X. Q. Guo, C. L. Fu, T. Wang, Z. Q. Wang and J. L. Li (2012), Petrology, geochemistry and SHIMP U-Pb dating of zircons from Late Triassic OIB-basalt in the conjunction of Qinling-Qilian-Kunlun orogens, *Earth Sci. Front.*, 19, 164–176.
- Yang, J.-H., S.-L. Chung, M.-G. Zhai, and X.-H. Zhou (2004), Geochemical and Sr-Nd-Pb isotopic compositions of mafic dikes from the Jiaodong Peninsula, China: Evidence for vein-plus-peridotite melting in the lithospheric mantle, *Lithos*, 73, 145–160.
- Yang, Y. H., H. Zhang, Z. Chu, L. Xie, and F. Y. Wu (2010), Combined chemical separation of Lu, Hf, Rb, Sr, Sm and Nd from a single rock digest and precise and accurate isotope determinations of Lu-Hf, Rb-Sr and Sm-Nd isotope systems using Multi-Collector ICP-MS and TIMS, *Int. J. Mass Spectrom.*, 290, 120–126.
- Yang, Y. H., Z. Y. Chu, F. Y. Wu, L. W. Xie, and J. H. Yang (2011a), Precise and accurate determination of Sm, Nd concentrations and Nd isotopic compositions in geological samples by MC-ICP-MS, *J. Anal. At. Spectrom.*, 26, 1237–1244.
- Yang, Y. H., F. Y. Wu, L. W. Xie, J. H. Yang, and Y. B. Zhang (2011b), High-precision direct determination of the 87Sr/86Sr isotope ratio of bottled Sr-rich natural mineral drinking water using multiple collector inductively-coupled plasma mass spectrometry, *Spectrochim. Acta B*, 66, 656–660.
- Yang, Y. H., F. Y. Wu, Z. C. Liu, Z. Y. Chu, L. W. Xie, and J. H. Yang (2012), Evaluation of Sr chemical purification technique for natural geological samples using common cation-exchange and Sr-specific extraction chromatographic resin prior to MC-ICP-MS or TIMS measurement, *J. Anal. At. Spectrom.*, 27, 516–522.
- Yaxley, G. M., and D. H. Green (1998), Reactions between eclogite and peridotite: Mantle refertilisation by subduction of oceanic crust, *Schweiz Mineral. Petogr. Mitt.*, 78, 243–255.
- Yu, X. H., X. X. Mo, Z. D. Zhao, W. Y. He, and Y. Li (2011), Cenozoic bimodal volcanic rocks of the West Qinling: Implication for the genesis and nature of the rifted north-south tectonic belt, *Acta Petrol. Sin.*, 27(7), 2195–2202.
- Zhang, C. L., T. Wang, and X. X. Wang (2008), Origin and tectonic setting of the Early Mesozoic granitoids in Qinling orogenic belt, *Geol. J. China Univ.*, 14(3), 304–316.
- Zhang, E. P., D. Y. Niu, Y. G. Hou, Y. G. Li and L. F. Zhang (1992), Geological map of Qinling-Daba Mountains and adjacent of the People's Republic of China, Geological Publishing House (In Chinese), Beijing.
- Zhang, G. W., B. R. Zhang, X. C. Yuan, and J. Y. Chen (2001), *Qinling Orogenic Belt and Continental Dynamics*, Sci. Press, Beijing.
- Zhang, H. F., L. L. Jin, L. Zhang, and N. Harris (2007), Geochemical and Pb-Sr-Nd isotopic compositions of granitoids from western belt: Constraints on basement nature and tectonic affinity, *Sci. China Ser. D*, 50, 184–196.
- Zhang, J.-J., Y.-F. Zheng, and Z.-F. Zhao (2009), Geochemical evidence for interaction between oceanic crust and lithospheric mantle in the origin of Cenozoic continental basalts in east-central China, *Lithos*, 110, 305–326.
- Zhao, Z.-F., L.-Q. Dai, and Y.-F. Zheng (2013), Postcollisional mafic igneous rocks record crust-mantle interaction during continental deep subduction, *Sci. Rep.*, 3, 3413, doi:10.1038/srep03413.
- Zheng, Y.-F. (2012), Metamorphic chemical geodynamics in continental subduction zones, *Chem. Geol.*, 328, 5–48.
- Zheng, Y.-F., W.-J. Xiao, and G.-C. Zhao (2013), Introduction to tectonics of China, *Gondwana Res.*, 23, 1189–1206.
- Zhu, L.-m., G.-w. Zhang, Y.-j. Chen, Z.-j. Ding, B. Guo, F. Wang, and B. Lee (2011), Zircon U-Pb ages and geochemistry of the Wenquan Mo-bearing granitoids in West Qinling, China: Constraints on the geodynamic setting for the newly discovered Wenquan Mo deposit, *Ore Geol. Rev.*, 39, 46–62.

## Erratum

In the originally published version of this article, the Ti content in Figure 4b is inconsistent with the data set in Table S2. Figure 4 was redrawn for better presentation of the Ti content in the primitive mantle-normalized trace element distribution patterns (Figure 4b). Figure 4 has since been corrected and this version may be considered the authoritative version of record.